Article

Current Biology

Long-range cortical synchronization supports abrupt visual learning

Highlights

- Monkeys rapidly learned to associate novel images with specific responses
- Simultaneously recorded neural activity from inferotemporal and prefrontal cortices
- Synchronization between these areas peaked around the moment of learning
- Coherence was strongest between image-encoding IT and reward-sensitive PFC sites

Authors

Bennett A. Csorba, Matthew R. Krause, Theodoros P. Zanos, Christopher C. Pack

Correspondence

bennett.csorba@mail.mcgill.ca

In brief

Using intracranial recordings in the macaque monkey brain, Csorba et al. investigate the neurophysiological bases of sudden improvements in performance during visual learning, often referred to as "moments of insight." Their data reveal a transient synchronization between prefrontal and visual cortices that occurs around the moment of learning.

Csorba et al., 2022, Current Biology *32*, 2467–2479
June 6, 2022
https://doi.org/10.1016/j.cub.2022.04.029

CellPress

Current Biology

CellPress

Article

Long-range cortical synchronization supports abrupt visual learning

Bennett A. Csorba,[1,3,*] Matthew R. Krause,[1] Theodoros P. Zanos,[2] and Christopher C. Pack[1]
[1]Montreal Neurological Institute, McGill University, Montreal, QC H3A 2B4, Canada
[2]Feinstein Institute for Medical Research, Manhasset, NY 11030, USA
[3]Lead contact
*Correspondence: bennett.csorba@mail.mcgill.ca
https://doi.org/10.1016/j.cub.2022.04.029

SUMMARY

Visual plasticity declines sharply after the critical period, yet we easily learn to recognize new faces and places, even as adults. Such learning is often characterized by a "moment of insight," an abrupt and dramatic improvement in recognition. The mechanisms that support abrupt learning are unknown, but one hypothesis is that they involve changes in synchronization between brain regions. To test this hypothesis, we used a behavioral task in which non-human primates rapidly learned to recognize novel images and to associate them with specific responses. Simultaneous recordings from inferotemporal and prefrontal cortices revealed a transient synchronization of neural activity between these areas that peaked around the moment of insight. Synchronization was strongest between inferotemporal sites that encoded images and reward-sensitive prefrontal sites. Moreover, its magnitude intensified gradually over image exposures, suggesting that abrupt learning is the culmination of a search for informative signals within a circuit linking sensory information to task demands.

INTRODUCTION

In adults, visual learning often requires prolonged training. Even for simple tasks, such as discriminating the orientation of a line, behavioral changes often emerge after days or weeks of practice.[1] For more complex tasks, such as the detection of anomalies in medical images, efficient performance requires months or years of training.[2,3] Neurophysiological studies have similarly revealed that the adult visual cortex often changes very slowly, if at all, in response to experience.[4,5]

At the same time, it is clear that adults are capable of rapid visual learning under right circumstances.[6,7] Indeed, learning can even occur following a single exposure to a stimulus[8] or abruptly after a series of unsuccessful attempts at a task.[6,7] This latter kind of learning, which Hebb referred to as "insight,"[9] has frequently been observed in freely behaving animals attempting to obtain reward in unfamiliar settings. These observations pose a challenge for modern theories of learning that rely on gradual synaptic changes following many presentations of the same stimulus.[10]

Abrupt learning would seem to be necessary for survival in natural visual environments, which typically do not afford the opportunity for hundreds of exposures to novel stimuli. At the same time, such plasticity must be engaged selectively, to prevent newly learned stimuli from overwhelming existing representations. One solution to this "stability-plasticity" dilemma is therefore to impose a gating mechanism, whereby abrupt visual learning occurs only when specific subgroups of neurons are active together.[9,11] For visual learning, the relevant subgroups might be those that encode the relevant stimuli and those that encode the demands of a given task or context.[12]

At a neural level, these operations can be implemented through oscillatory synchronization, which has been shown to support the rapid formation of new memories,[13–15] as well as long-range communication more generally.[16] It has also been implicated in functions that are important for slower forms of learning, such as attention[1] and reward sensitivity.[14] Critically, oscillatory synchronization can change flexibly on short timescales so as to link different brain regions that contain different types of task-relevant information.[11] However, the role of this kind of synchronization in abrupt visual learning is unknown.

Here, we have tested the hypothesis that oscillatory synchronization facilitates rapid visual learning using multi-site neural recordings in non-human primates. The animals were trained to perform a naturalistic "foraging" task, in which they learned to recognize a visual image and to associate it with a rewarded location. Learning in this task was abrupt, with most sessions being characterized by large performance improvements over the course of a few trials. At the same time, we recorded from the prefrontal cortex (PFC) and inferotemporal (IT) cortex, which are known to interact during visual learning and perception.[17–19]

Around the "moment of insight," we found a transient increase in synchronization between neural activity in these two cortical areas. This increase in synchronization was strongest between prefrontal sites that encoded reward and IT sites that discriminated between the relevant visual stimuli. In contrast, we did not find local changes in neural firing or oscillatory power that correlated strongly with learning. Therefore, these results suggest that rapid learning relies on temporal synchronization between cortical sites that connect relevant stimuli with task outcomes.

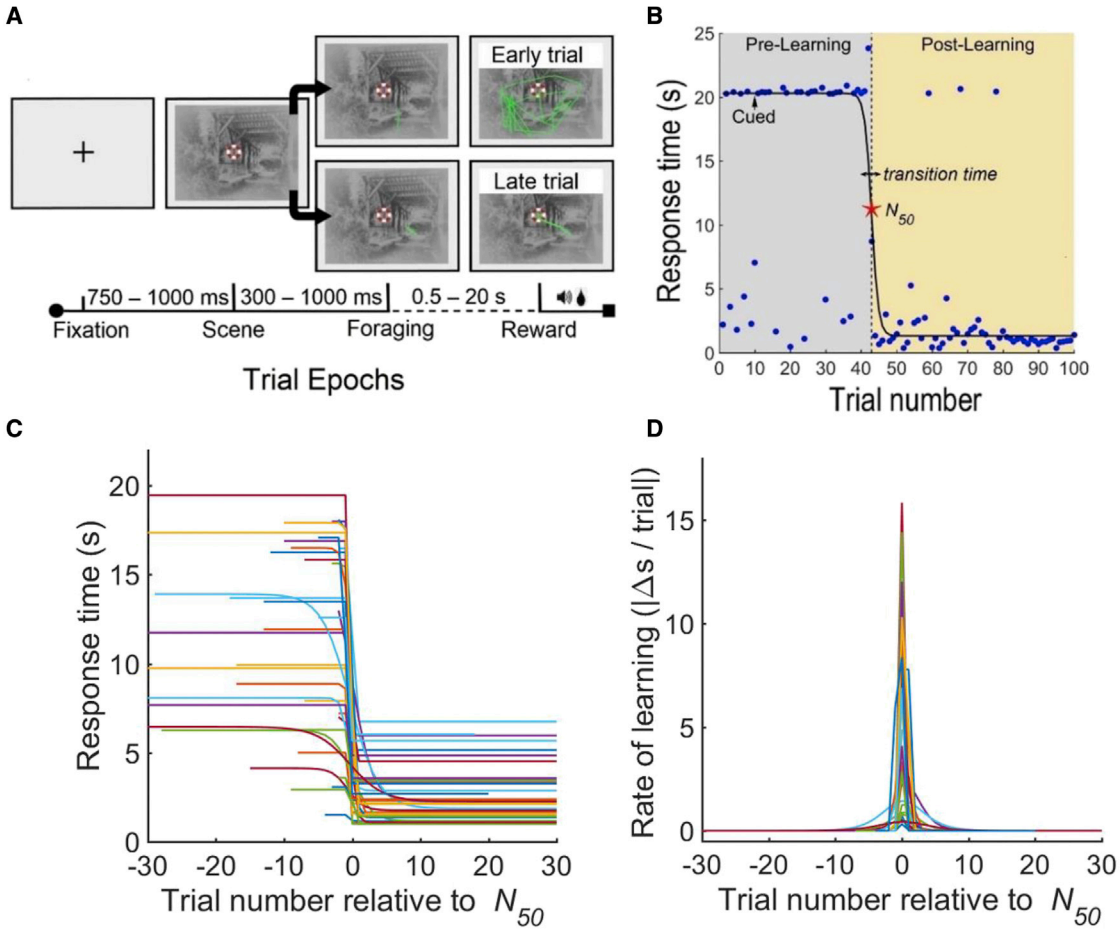

Figure 1. Task diagram and behavior

(A) An oculomotor "foraging" task was used to study visual learning. Each trial began with the onset of a fixation cross. After fixation was acquired, a natural image appeared, and animals were then free to explore the image in search of a reward zone (red-white ring but not visible to the subject). Fixation on the reward zone led to the release of the reward and the end of the trial. If the reward zone was not found after 15 s (monkey F) or 20 s (monkey M), a cue indicated the rewarded location. Eye traces (green) are shown for an example early trial (top), when the animal failed to find the reward zone after 20 s, and a late trial (bottom), after learning was complete. The two images were shown in an interleaved manner in every session.

(B) Behavioral performance for an example image. Blue dots indicate the time required to find the target on a single trial, and the black line indicates the fit of a sigmoid function to the data for all trials. The red star indicates the N_{50} trial, estimated from the sigmoid fit as the time required for performance to improve by 50% from its pre-learning to its post-learning state.

(C) Sigmoid fits for all images for monkey M, aligned on the N_{50} value for each image. Fits for monkey F are included in Figure S1E.

(D) The rate of learning, defined as the performance change as a function of trial, for images for monkey M, aligned on the N_{50} value for each image. Data for monkey F are included in Figure S1F.

See also Figure S1.

RESULTS

Abrupt visual learning in a naturalistic behavioral paradigm

To probe the mechanisms of abrupt learning, we used the "oculomotor foraging" task shown in Figure 1A.[20,21] On each trial, animals freely explored a natural scene until their gaze landed within an unmarked reward zone (RZ). A fixation within the RZ triggered the release of a few drops of juice and ended the trial. Both the starting eye position and the precise location of the RZ varied from trial to trial (STAR Methods) so that animals could not perform the task by simply associating a fixed saccade vector with each image (Figures S1G–S1L). Instead, they had to learn the spatiotopic location of the RZ within the image.

Within each session, animals were exposed to two different images, each with its own unique RZ, in a randomly interleaved fashion. Visual learning was therefore an important component of the task, as both the images were initially unfamiliar to the animals.

Figure 1B shows the progression of learning within a single example session, considering only one of the two images presented. Each point shows the response time,[21] defined as the time it took the animal to find the RZ on each trial. Although the animal occasionally found the RZ quickly, typical response times were initially very high. This was not due to a lack of

engagement, as the animal actively searched the image, making on average 41.5 saccades on each trial (Figure S1B). To maintain engagement during the early pre-learning phase, these trials timed out after 15 or 20 s, at which point a cue was shown to provide a hint about the correct location (Figure 1A, top).

On the 43rd trial for this example image, a moment of insight occurred and the typical response time abruptly dropped from 20 to ~1 s. Response times then remained low in most subsequent trials, suggesting that the animal had successfully learned to recognize this image and to associate it with the corresponding RZ. Overall task engagement appeared to be similar before and after learning as the animals continued to generate saccades at similar rates (Figure S1B; 3.69 ± 0.27 versus 3.29 ± 0.21 saccades/s). However, after learning, the saccades were generally directed toward the RZ, resulting in trials of shorter duration.

To quantify the dynamics of learning, we fit the sequence of response times for each image to a sigmoid function (the solid line in Figure 1B). From the sigmoid fits, we extracted two quantities (STAR Methods). The first was N_{50} (the red star in Figure 1B), defined as the trial in which response time decreased by half from its initial value—we used this value as an objective marker of the trial for which learning was centered. The second was the transition time (the arrow in Figure 1B), defined as the number of trials required for performance to go from 75% to 25% of the maximum response time indicated by the sigmoid fit. For the data shown in Figure 1B, the transition time was two trials, which lasted 10.1 s in total, indicating that learning was indeed abrupt.

In total, we obtained behavioral and electrophysiological data from sessions involving 50 different images (37 from monkey M and 13 from monkey F). As in the example, the behavioral data were well fit by a sigmoid function (median $r^2 = 0.76$), with the fit quality not differing significantly between the two animals (one-way ANOVA, $p = 0.59$). From these fits, we estimate that the median value of N_{50} was 18 trials and the mean transition time was 1.58 trials (SE = 0.15 trials). Basic eye movement metrics including saccade rate, microsaccade rate, and latency to the first saccade on each trial did not vary significantly with learning or between subjects (two-way ANOVAs, $p > 0.05$).

Figures 1C and 1D summarize the progression and rate of learning for all images for an individual animal (monkey M). As in the example session, performance changes were confined to a few trials around the N_{50} trial for each image. Similar results for the second animal are shown in Figures S1E and S1F. Overall, these results show that learning had a pronounced effect on task performance, it happened rapidly, and it usually followed a prolonged period of unsuccessful task performance. These characteristics are typical of abrupt learning.[6,9]

We also verified that this learning was persistent, by retesting the animals on a subset of the images, many days after the first exposure. On average, response times during the first 10 trials for each image decreased by 1.90 s from the first session to the retest session, and the N_{50} value decreased by 12.6 trials (two-way ANOVAs, by session, $p < 0.05$, for animal or session × animal interaction, $p > 0.05$). Even before N_{50}, the animals consistently made fewer saccades during recall sessions than in the initial sessions (two-way ANOVA, $p < 0.05$), indicating that they retained a memory of the images. Thus, our foraging paradigm led to abrupt learning that was quite durable, as has been reported for other abrupt learning tasks[22] and for learning in the wild.[23]

Cortical dynamics of abrupt learning

To assess the cortical basis of abrupt learning, we recorded simultaneously from 96-channel electrode arrays in IT and PFC (Figure 2). Area IT is known to be important for recognizing complex images,[24] whereas PFC plays a role in learning arbitrary associations.[25] Lesion studies have suggested that the connections between these two areas are especially important for learning associations between images and spatial locations,[19,26] but the physiological nature of this interaction is unknown.[27] We therefore examined the functional interactions between sites in IT and PFC to determine how they evolve with learning.

To focus our analysis, we defined three epochs during each behavioral trial. As shown in Figure 1A, these are the "scene onset" epoch, when the image first appeared; the "foraging" epoch, when the search was initiated; and the "reward" epoch, when the reward was dispensed. These were chosen because retinal stimulation was largely identical within each epoch throughout the progression of learning (STAR Methods). To characterize learning-related changes in synchronization between PFC and IT, we examined the oscillatory coherence between the local field potential (LFP) signals in each area, a commonly used metric that indexes transient changes in corticocortical communication during learning[28,29] (STAR Methods).

To illustrate the general pattern of results, Figure 3A shows the magnitude of synchronization between the two areas, averaged across electrodes and images for both animals. Here, we have grouped trials into a pre-learning phase (before N_{50}, top row), a post-learning phase (after N_{50}, bottom row), and those around the moment of abrupt learning (N_{50}, middle row). The left column, corresponding to the scene onset epoch, shows that the appearance of a visual image generally triggered an increase in low-frequency synchronization starting around 200 ms later. This sensory response was consistent throughout the progression of learning (two-way ANOVA, either learning phase or by animal or the interaction, $p > 0.05$).

In contrast, the onset of the foraging epoch (middle column) was accompanied by an increase in gamma band (30–50 Hz) synchronization, which was most prominent around the N_{50} trial, when learning was most evident (middle row). A Granger-Geweke causality analysis revealed that the timing of these oscillations was consistent with a feedforward flow of information from IT to PFC (two-way ANOVA, $p < 0.05$ for the main effect of direction and $p > 0.05$ for the animal). Similarly, the receipt of the reward (right column) was accompanied by a strong increase in alpha band (8–12 Hz) synchronization that was localized to the trials near N_{50}. This synchronization was more consistent with feedback transmission (ANOVA, $p < 0.05$ for direction and $p > 0.05$ for the animal). These two synchronization events were the strongest candidates for a neural correlate of the moment of insight in our data.

Indeed, across sessions, synchronization between IT and PFC accurately predicted changes in behavioral performance. As shown in Figures 3B and 3C, there was a strong correlation between the trials at which synchronization peaked and the behavioral N_{50} trials ($r^2 = 0.62$ for gamma synchronization in the foraging epoch and $r^2 = 0.73$ for alpha synchronization in the reward epoch,

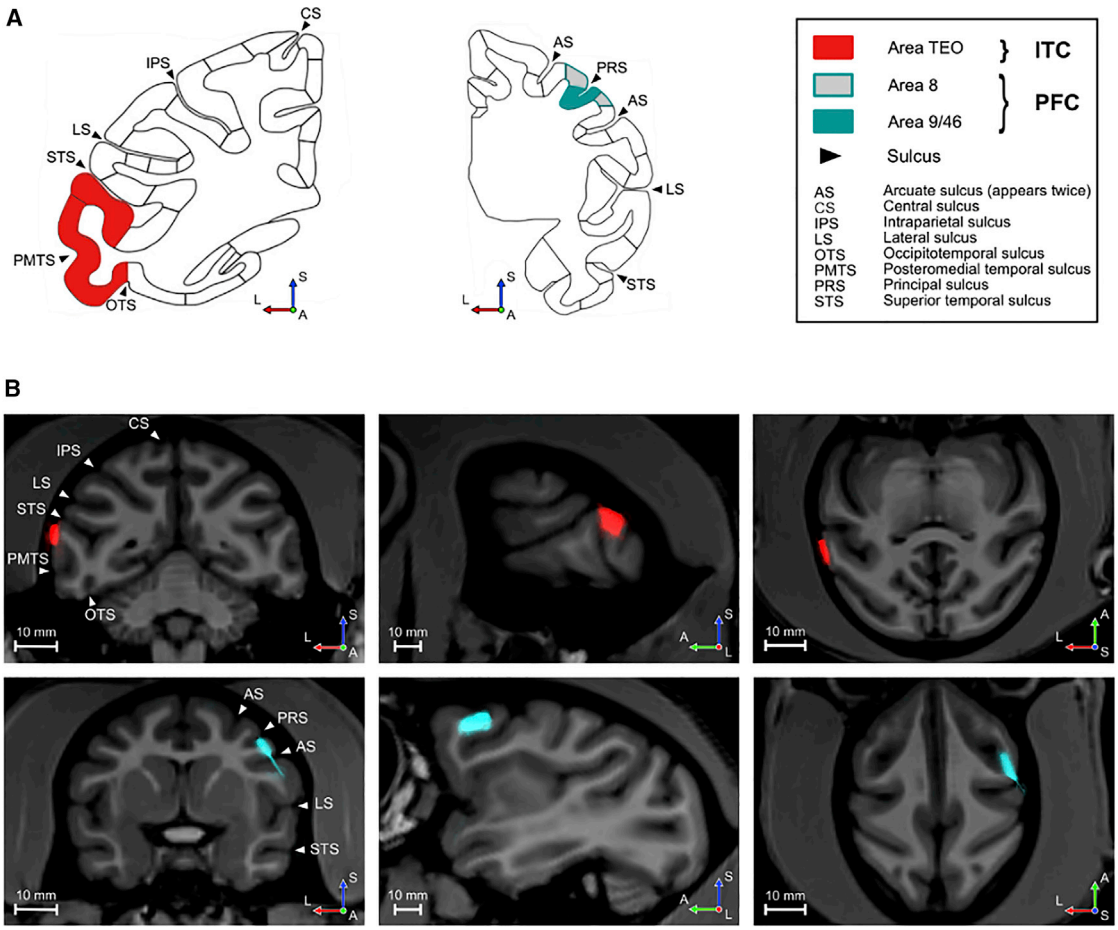

Figure 2. Electrode array locations (monkey F)

Images are shown in neurological convention ("left is left"). L is left, A is anterior, and S is superior.

(A) Coronal sections from the Markov et al. CoreNets atlas30 showing the brain areas targeted for recording. The sulcal landmarks indicated were used to identify the same regions in each animal's MRI. Due to its curved shape, the arcuate sulcus (AS) appears twice in the coronal PFC sections.

(B) Combined MRI/CT images showing the positions of IT (top row) and PFC (bottom) arrays in coronal (left), sagittal (center), and axial (right) planes. The preoperative T_1-weighted MRI was co-registered with a postoperative CT scan (red and cyan) to verify the array locations. To emphasize the neuroanatomy, the skull and artifacts from other implants have been digitally removed from the CT scan.

Pearson correlation tests, $p < 0.05$, corrected). These associations were significant for each animal individually (linear regression, trial $\sim N_{50}$, $p < 0.05$, corrected) and when the data were combined across animals (linear regression, trial $\sim N_{50}$, $p < 0.05$, corrected). In contrast, the absolute magnitude of the change in synchronization did not predict the behavioral moment of learning for either frequency band or epoch (two-way ANOVAs, $p > 0.05$).

Moreover, the trials with peak alpha synchronization were correlated with the trials with peak gamma synchronization ($r^2 = 0.72$ and $p = 0.008$), indicating that both signals were present for individual images within the same sessions (Figure S1C). Notably, we were unable to detect a timing difference between the trial of peak gamma synchronization in the foraging epoch and the trial of peak alpha synchronization in the reward epoch (Wilk test, $p > 0.05$).

In contrast, for images that the animals failed to learn (see STAR Methods for criteria), there was little change in synchronization across trials (two-way ANOVAs, $p < 0.05$). Thus, abrupt learning was associated with an increase in gamma synchronization in the foraging epoch and an increase in alpha synchronization in the reward epoch, both of which appeared to be highly specific to a moment of insight. We therefore focus on these two signals in the following sections.

Selection of sensory signals during abrupt visual learning

To perform the foraging task, the animals had to recognize which of the two images was present on each trial before responding with the appropriate eye movements. According to the hypothesis outlined in the introduction, learning to recognize images should correspond with oscillatory synchronization that is specific to the sites that encode the relevant stimuli. These sites are most likely found in IT subpopulations that are selective for the images shown in each session.

To test this hypothesis, we first trained a decoder to discriminate between the two images presented in each session, using linear discriminant analysis (LDA; STAR Methods). The decoder was trained on multi-unit activity in IT and recorded during the

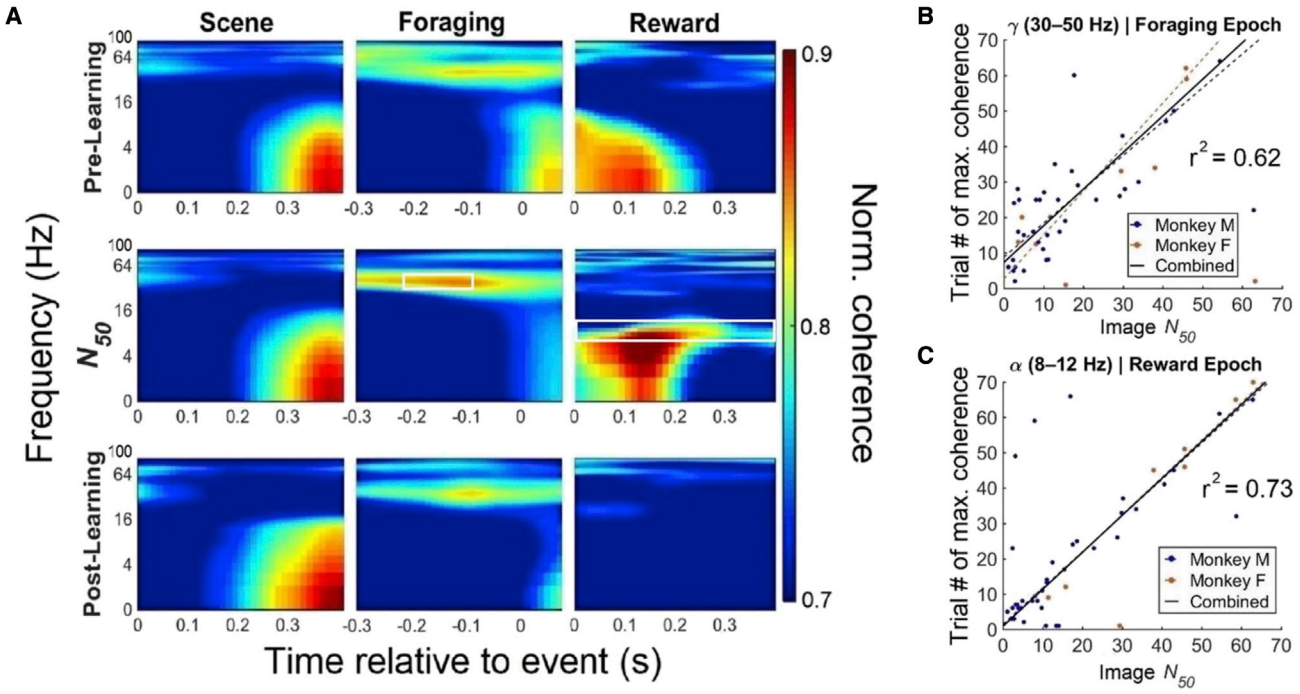

Figure 3. Inferotemporal-prefrontal oscillatory synchronization reflects the learning state

(A) Synchronization of the LFP signals between IT and PFC is shown for the three-trial epochs (scene, foraging, and reward) at different stages of learning (pre-learning, N_{50}, and post-learning). Each panel contains a time-frequency plot covering frequencies in the range of 1–100 Hz and a period of 400 ms around the event that defines each epoch. The time-frequency regions of interest selected from these preliminary data are indicated in white. Around the moment of learning, there was a notable increase in gamma (30–50 Hz) synchronization in the foraging epoch (middle column, middle row, two-sided permutation t tests, $p < 0.05$) as well as increased alpha band (8–12 Hz) synchronization during the reward epoch (right column, middle row, two-sided permutation t tests, $p < 0.05$) relative to pre-learning activity.

(B) Trial number of peak gamma synchronization (30–50 Hz) in the foraging epoch is plotted against the N_{50} value from the sigmoid fit for the corresponding behavioral data, for each monkey separately (red and blue dots), along with best-fitting regression lines for each animal (red and blue dashed line). The black line indicates the best-fitting regression line for all data combined.

(C) Same as in (B) but for alpha synchronization during the reward epoch.

scene onset epoch. This approach provides a close correlation of perceptual discriminability in other contexts.[30] Consistent with the importance of visual recognition for the task, more difficult image discriminations required more trials to learn—decoding performance was negatively correlated with the number of trials required to reach N_{50} ($r = -0.48$, Pearson correlation test, $p = 0.004$).

To probe the cortical dynamics of this learning, we used the weights recovered from the LDA to rank each IT electrode according to the selectivity of its multi-unit activity for the two images in each session. These weights provided a measure of informativeness—sites that were assigned high weights in the LDA were necessary for the population to discriminate between the two images, whereas those with low weights were not. From this analysis, we ranked IT electrodes from most informative to least informative in each session.

Figure 4 shows the average strength of interareal synchronization relative to the N_{50} trial, computed in a moving window of five trials (STAR Methods) and averaged across images—data from the example image in Figure 1 are shown in Figure S1D. For visualization purposes, we first focus on the 10 most and 10 least selective IT electrodes, but as shown below (Figure 6), the results are not specific to this choice.

For gamma oscillations in the foraging epoch (Figures 4A and S3G), the synchronization between PFC and IT was initially similar, regardless of the informativeness of the IT electrodes. That is, early in the session, synchronization strength was similar for the most informative (red) and least informative (blue) IT electrodes. However, for later trials, the most informative IT electrodes became significantly more synchronized with PFC (Figure S3G) compared with the least informative IT electrodes. A two-way ANOVA revealed a significant effect of informativeness ($p < 0.05$) but no difference between animals and no interaction between these factors ($p > 0.05$, corrected). Interestingly, this synchronization peaked near the N_{50} trial (Figure 4A), after which synchronization between IT and PFC decreased gradually, with the preference for informative IT electrodes also becoming weaker. Similar results were obtained for the alpha band (Figure S3E; two-way ANOVA, $p > 0.05$) and the gamma band (Figure S3F; two-way ANOVA, $p < 0.05$) when we instead analyzed the LFP before the final saccade of each trial.

A similar pattern was seen for alpha synchronization during the reward epoch (Figures 4B and S3G). Synchronization with PFC was initially similar across IT electrodes, but as trials progressed, the strength of synchronization increased for the most

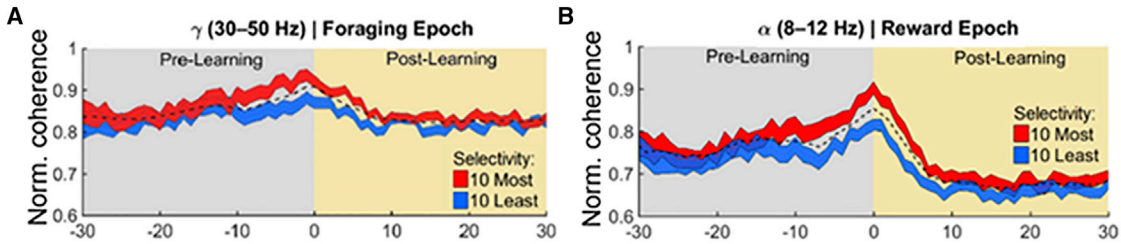

Figure 4. Image-selective sites in the IT drive synchronization around the time of learning

(A) Synchronization between IT and PFC is shown for the gamma band (30–50 Hz) in the foraging epoch. Here, data have been averaged across time within an epoch and across images. Results are aligned on the N_{50} trial for each image. The dashed black line represents the grand median of all usable electrode pairs for all sessions. The red and blue lines correspond to the average strength of synchronization between all PFC sites and those IT sites that are most (red) and least (blue) informative about the images shown in each session. The shading around each line indicates the SEM.

(B) Same as in (A) but for alpha synchronization (8–12 Hz) during the reward epoch.

See also Figures S1–S3.

informative IT electrodes, both in absolute terms and relative to the least informative electrodes (two-way ANOVA, by informativeness, $p < 0.05$, for animal or informativeness × animal interaction, $p > 0.05$, corrected). Here, a distinct peak in synchronization was also evident around the N_{50} trial, with a strong preference for informative IT electrodes. This preference also diminished after learning was complete, but it did not disappear entirely, as the increased contribution of informative IT sites to alpha synchronization persisted throughout the post-learning period (two-way ANOVA, $p < 0.05$, for animal or informativeness × animal interaction, $p > 0.05$, corrected). Similar results were evident when data for each animal were analyzed independently (Figures S2E and S2F). Thus, both gamma and alpha synchronization peaked around the N_{50} trial, and long-range synchronization levels were significantly stronger for image-selective IT sites. This suggests that learning was associated with a selective flow of sensory information in both the feedforward and feedback directions.

From Figure 4A (and Figure 4B), it is also apparent that the selective contribution of different groups of IT electrodes to interareal synchronization began on average well before the N_{50} trial. Statistically, the increased gamma synchronization of the most informative IT electrodes compared with the least informative IT electrodes began 10 trials before the N_{50} trial (Figure S3H). For alpha oscillations, the difference emerged 14 trials before the N_{50} trial (Figure S3G). Thus, even considering that our analysis had a resolution of five trials (STAR Methods), it appears that the selective synchronization of sensory signals began on average well before the behavioral moment of learning. Presently, because our analysis averages across sessions and trials, we cannot precisely quantify how abruptly or gradually this synchronization occurs.

These findings indicate that abrupt learning at the behavioral level might be caused by synchronization of image-selective IT sites with PFC. The alternative possibility, that synchronization with PFC causes image selectivity to develop in IT, was not consistent with our data, as synchronization levels measured before learning did not predict decoding accuracy or electrode informativeness in IT, for either epoch (two-way ANOVAs, $p > 0.05$). Thus, although a conclusive test will require causal perturbations,[31] the data favor an influence of stimulus selectivity on synchronization.

This arrangement could arise trivially if unresponsive IT electrodes were included in the analysis. Unresponsive electrodes would be neither synchronized with PFC nor selective for images, so they could exaggerate or even cause the association between synchronization and selectivity, as shown in Figure 4. To control for this possibility, we recomputed the synchronization analysis shown in Figure 4 after sorting the IT electrodes based on the responsiveness of their MUA signals (Figures S2C, S2D, S3A, and S3B) rather than their selectivity. Responsiveness was defined as the change in MUA firing rate in the 400 ms following the release of the reward.

In contrast to the results shown in Figure 4, there was no difference in the synchronization between strongly responsive and weakly responsive IT sites (two-way ANOVA, $p > 0.05$), indicating that it is image selectivity, rather than signal quality, that drives synchronization changes during learning. Consistent with this idea, the most (and least) informative electrodes changed from session to session (Figure S2A), which would not occur if defective electrodes were included in the analysis. Moreover, image selectivity by itself did not account for synchronization in other trial epochs or frequency bands (Figures S3C and S3D).

We conclude that abrupt learning was associated with a gradual increase in synchronization between the PFC and IT sites that carried the most information about the visual stimuli. These changes were specifically related to IT selectivity, as no similar pattern was found when electrodes were sorted according to image selectivity or responsiveness in PFC (Figure S4). Thus, although previous work has found evidence of visual selectivity in PFC,[32] this selectivity does not appear to be relevant for abrupt learning in our task.

Contribution of reward signals to abrupt visual learning

Although informative sensory signals are necessary for our task, they are not sufficient, as the image identity must be linked with its corresponding RZ. The hypothesis outlined in the introduction therefore suggests that abrupt learning might require informative sensory signals to become synchronized with neural sites that carry information about the reward context for each image.

To test this possibility, we first asked whether the location of the RZ was encoded in the neural responses in PFC. Previous work has shown that some PFC neurons respond selectively to rewarded stimuli when they are placed in specific spatial

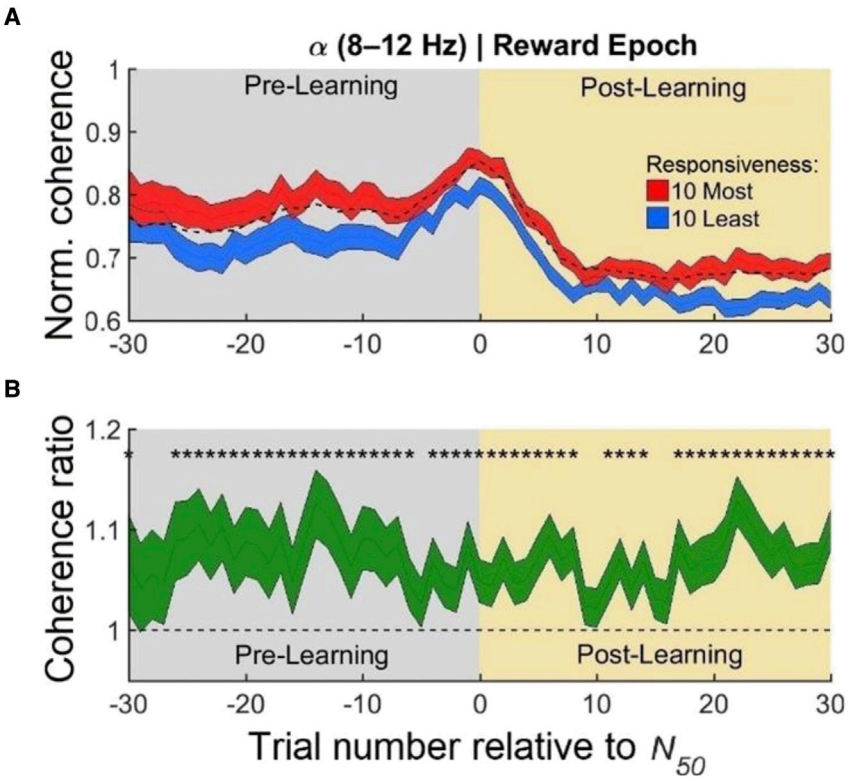

Figure 5. Reward-responsive sites in PFC are more synchronized with sites in IT

(A) Synchronization between IT and PFC is shown for the alpha band (8–12 Hz) in the reward epoch. Conventions as in Figure 4. The shading around each line indicates the SEM.

(B) The ratio of IT-PFC synchronization strength between reward-responsive and unresponsive PFC electrodes. Asterisks indicate a ratio significantly different from 1.

See also Figures S2, S4, and S7.

locations,[33] so we recorded MUA responses during interleaved trials in which animals had to make a visually guided saccade to receive a reward (STAR Methods). For these trials, there was no learning and no visual stimulation other than the saccade target. We then sorted the PFC electrodes according to their preference for the location of the RZ over opposite spatial locations (Figure S7I; STAR Methods).

The sites that responded selectively to the position of the RZ were generally not more coherent with IT electrodes, in either epoch or frequency band (Figure S7). This was the case whether we defined the RZ position in retinal coordinates (relative to the fixation point on each trial) (two-way ANOVA, either retinal coordinates or by animal or the interaction, $p > 0.05$) or in screen coordinates (two-way ANOVA, either screen coordinates or by animal or the interaction, $p > 0.05$). A similar lack of RZ encoding was found in IT (Figure S7; two-way ANOVAs, $p > 0.05$). Thus, it does not appear that the sites from which we recorded play a role in maintaining the location of the RZ.

An alternative possibility is that learning in our task relies on a non-specific reward signal, as suggested by some computational models.[34] Indeed, a population of neurons in PFC encodes reward, independently of its associated target location,[33] and these neurons would seem to be well suited to carry out this role. We therefore asked whether PFC sites that are sensitive to reward[35] play a role in abrupt learning.

Figure 5 shows the LFP synchronization between PFC and IT, with data again averaged across images relative to the N_{50} trial, as in Figure 4. However, in this case, the PFC electrodes have been sorted according to the responsiveness of their MUAs to the release of the reward (STAR Methods). For alpha oscillations during the reward epoch, the most reward-sensitive (red) PFC sites exhibited greater synchronization with IT than the least reward-sensitive PFC sites (blue) (two-way ANOVA, by responsiveness, $p < 0.05$, for animal or responsiveness × animal interaction, $p > 0.05$, corrected). In contrast to the results shown in Figure 4, this increased synchronization was not aligned on the N_{50} trial but rather appeared to be a non-specific signal that persisted across the duration of each session. Furthermore, in contrast to the IT results, the electrodes that provided this reward signal were consistent from image to image (Figure S3B), as would be expected based on the anatomical organization of reward signals in PFC.[35] This effect was again not due to poor electrode quality, as there was no similar preferential synchronization for other frequencies and epochs (Figure S4).

The full interaction between reward and sensory signals is shown in Figure 6, for all sites in both areas. Here, each panel corresponds to the data averaged across images for trials relative to the N_{50} trial. As in Figures 4 and 5, the IT electrodes have been ranked according to their informativeness about the images in each session, and this ranking is indicated on the x axis of each panel. The PFC electrodes have been ranked according to their responsiveness to reward, and this ranking is indicated on the y axis of each panel. The color at each point in each map indicates the average strength of synchronization between electrodes of the corresponding ranks. The reddish colors indicate strong synchronization, and the bluish colors indicate weak synchronization.

For the trials near N_{50} (Figure 6A, center panel), the strongest alpha synchronization is indeed limited to image-selective sites in IT and reward-sensitive sites in PFC. This is shown by the concentration of reddish colors in the upper right of the panel—the contour plot in Figure 6B emphasizes that the strongest synchronization occurs between these same subpopulations. For trials long before or after the N_{50} trial, synchronization is generally weaker and distributed more diffusely across sites in both areas. These findings were stable across recording sessions (Figure S2J; $R^2 = 0.05$ and $p = 0.09$).

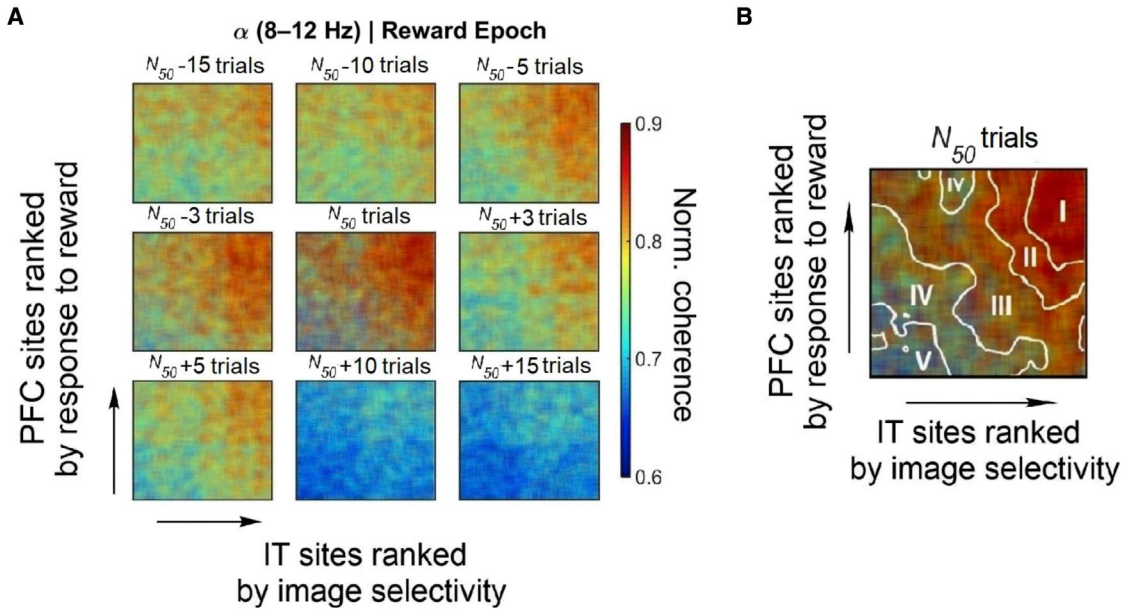

Figure 6. Interaction of reward-responsive sites in PFC and image-selective sites in IT

(A) Alpha synchronization in the reward epoch for all IT and PFC electrodes across sessions. Reddish colors indicate strong synchronization, whereas the bluish colors indicate weak synchronization. Different panels correspond to different trials relative to the N_{50} trial. Electrodes in IT were ranked based on how much information they carried about images within each session (increasing informativeness from left to right). Electrodes in PFC were ranked based on how strongly they responded following a reward (increasing sensitivity from left to right). Synchronization is generally weak and lacks organization early in each session (top left) but grows stronger around the moment of learning (central panel).

(B) Synchronization around N_{50} is clearest between the IT electrodes that encode images and the PFC electrodes that encode reward (top right of central panel). Data were placed into quintiles according to synchronization strength, and contours were drawn between levels to illustrate this synchronization structure.

See also Figure S2.

(Lack of) local correlates of abrupt learning

The results thus far indicate that synchronization between IT and PFC is a strong correlate of abrupt learning. For slower forms of learning, previous work has found changes in selectivity at the single-neuron level in both IT[36,37] and PFC.[17] We therefore looked for similar changes in each area that might reflect abrupt learning.

We used the decoding approach outlined above to assess whether multi-unit population activity showed improved discrimination ability with learning. The decoders were trained on the same images during the scene onset epoch for the pre-learning, peri-learning, and post-learning stages of each session. The results reveal that image decoding performance was generally strong in both areas, with the mean cross-validated classification rates being 87.5% (SE = 2.46%) in IT and 76.3% (SE = 1.72%) in PFC. However, decoding performance did not change with learning, in either IT or PFC (Figure 7A). Moreover, we did not find differences in average multi-unit firing rates between the pre-, peri-, and post-learning periods in either area for either animal (Figure 7B) (t tests, $p > 0.05$, corrected). In fact, the pattern of population activity in each area did not change significantly across learning epochs (two-way ANOVAs, $p > 0.05$). Thus, it does not appear that neural population activity became more selective or responsive to the images during abrupt learning.

Similarly, there was no consistent change in the LFP power (Figures S6A and S6B) or intra-areal synchronization (Figures S6C and S6D) around the moment of learning, either globally per area or when electrodes were sorted by informativeness in any frequency band for either animal (t tests, $p > 0.05$, corrected). In IT, there was a weak negative correlation between image selectivity and both alpha ($r^2 = 0.03$, Pearson correlation test, $p < 0.01$) and gamma ($r^2 = 0.04$, Pearson correlation test, $p < 0.01$) LFP power (Figures S6E and S6F). Finally, the IT electrodes' responses to reward did not change with learning in a way that was either frequency-specific or specific to their informativeness about the image (t tests, $p > 0.05$, corrected).

Across trials, there was however a steady decrease in the overall PFC power and intra-areal coherence. Similar results have been reported previously, and it has been suggested that they might reflect a weaker[38] or more selective engagement with sensory information as learning progresses. The latter possibility is consistent with the finding that overall synchronization often decreases after learning (Figure 4), although the relative advantage for image-selective sites persists (Figures S3G and S3H). A similar conclusion has been reached from fMRI studies of learning.[39]

DISCUSSION

Visual learning has traditionally been studied in laboratory tasks that involve extensive training to associate specific stimuli with specific responses. Such training can profoundly alter the underlying cortical circuitry,[40] but it does not necessarily reflect the kind of learning that occurs in natural settings. We have therefore examined learning in a more naturalistic, free-viewing task that

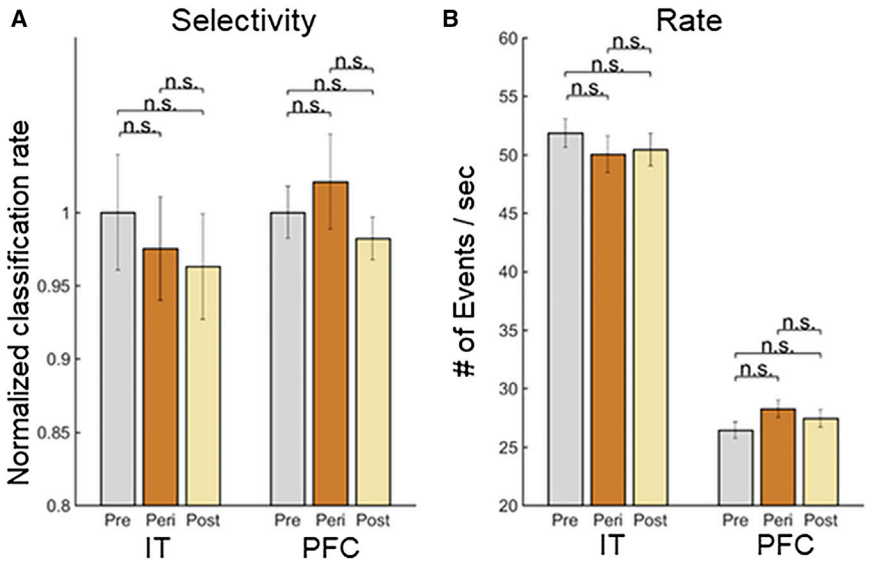

Figure 7. Learning does not affect multi-unit population firing activity or selectivity

(A) Selectivity of multi-units for scenes was assessed with a linear discriminant analysis (LDA). Neural data were split into pre-learning (gray), peri-learning (bronze), and post-learning epochs (yellow) for each image, using the sigmoid fits described in Figure 1 and the STAR Methods. Selectivity levels in the IT or PFC did not, on average, improve between learning epochs. The error bars reflect the standard error (SE) across sessions.

(B) Similarly, learning did not result in changes in responsiveness between the learning epochs.

See also Figures S5 and S6.

approximates the kind of foraging that primates perform daily in the wild. This behavior is thought to have driven the evolutionary expansion of PFC as well as its connection with IT.[41]

We found that non-human primates engaged in our foraging task abruptly learned to recognize visual images and associate them with specific reward locations (Figure 1). The strongest neuronal correlates of this learning were found in the synchronization of the LFPs between PFC and IT (Figure 3), and this synchronization seems well suited to link informative visual inputs with signals about rewarded outcomes (Figures 4 and 5). The strength of this synchronization was greatest around the moment of insight (Figures 4 and 5), but the tendency for informative IT signals to be more synchronized with PFC persisted well into the post-learning phase of each session (Figure 4). Local correlates of learning were largely absent in both IT and PFC (Figure 7). These results therefore indicate that long-range synchronization is capable of supporting abrupt visual learning.

Theories of abrupt learning

Hebb was among the first to evince a theory of abrupt learning, hypothesizing that the underlying neurophysiological mechanisms share some properties with those that support learning on longer timescales.[9] More recent work has provided some support for this idea by showing that rapid learning exhibits stimulus specificity similar to that observed with slower learning.[6,42]

Computational work has explained both types of learning based on a process in which decision-making structures search for the most informative sensory neurons for a given task.[43,44] This proposition is entirely consistent with the current results (Figure 4), as well as previous findings in other brain regions.[40,45] Moreover, in accordance with psychophysical results, we find that the selection of informative sensory inputs relies on explicit feedback[42] in the form of reward.

The mechanism by which reward signals are connected to informative sensory signals is likely related to that of top-down attention, which is important for most kinds of learning.[1] The interplay of these different kinds of feedback is captured effectively by models that typically operate on longer timescales.[46] In these models, a successful trial (i.e., one followed by reward) is followed by an attentional signal that selectively targets the upstream neurons that led to the rewarded outcome.

Role of oscillations in abrupt learning

Hebb's favored mechanism for learning took the form of cell assemblies that become connected after being repeatedly activated at the same time. Modern investigations of this hypothesis in humans have confirmed that long-range synchronization between different brain regions is a reliable correlate of certain kinds of learning.[47,48] This coherence has often been found in the gamma band,[13,47] which is also associated with learning in our task (Figures 3 and 6). Although the relationship between gamma oscillations and learning was correlational in this work, there is some evidence for a causal connection as well.[21,49]

We found that alpha synchronization seemed most related to the release of reward within each trial (Figure 5). This makes sense in light of previous findings, in which alpha oscillations in PFC are modulated by dopaminergic signals arriving via the striatum.[50] Indeed, blocking dopamine receptors in PFC impairs associative learning and alters alpha oscillations, and as a result, it has been suggested that alpha plays a role in controlling neural selectivity for sensory inputs.[50] More generally, alpha is commonly thought to gate neural activity according to task demands.[51]

Abrupt learning in the prefrontal cortex

Most previous work has suggested that PFC plays a role in facilitating learning but that it is not itself the primary site of long-lasting plasticity.[52,53] Instead, it might be involved in discerning the rules that map stimuli to responses for a given task.[54] The encoding of these rules can appear abruptly in PFC for novel associations[55] or for reversals of previously learned associations.[56] However, learned improvements in stimulus encoding are less common, and there is even evidence that stimulus encoding decreases with learning,[38] suggesting that PFC likely does not learn novel stimuli on short timescales. Our results (Figures 3 and 4) are consistent with this idea, since there is little evidence of enduring changes in image selectivity in the PFC neurons we recorded (Figure 7).

For visuomotor associations, the connection between PFC and IT is known to be critical.[19] Lesions that disconnect these areas severely impair visuomotor learning and especially "object in place" learning, a kind of rapid learning that resembles our foraging paradigm.[19] A more mechanistic role for PFC is suggested by the finding that neurons in this area help to solve the "credit assignment" problem. This refers to the challenge faced by the brain in identifying synaptic connections that can be strengthened to improve performance on a given task. Asaad et al. reported that selective visual signals were found in populations of PFC neurons that also represented reward outcomes, as would be necessary to solve the credit assignment problem.[57] Our results suggest that this information emerges dynamically through communication between subpopulations of IT neurons that encode the relevant stimuli and PFC neurons that encode the reward (Figure 6).

Abrupt learning in the visual cortex

While previous work has found rapid learning in individual IT neurons,[37,58] we did not find evidence for this at the population level (Figure 7). One possibility is that learning affected different classes of neurons differently,[59] which would not have been reflected in our population-level results, as we do not have a reliable way of assessing molecularly defined cell types in our sample.

With extended training, changes in neural selectivity have been observed in IT,[60,61] V4,[62,63] V2,[4] and V1.[5] These results are generally consistent with the observation that the adult visual system changes quite slowly with training.[1] Far less is known about the effects of rapid learning in the visual cortex, but Wang and Dragoi reported a transient, learning-related increase in spike field coherence in area V4.[64] This coherence increase was found in the theta band and within a single area but followed a similar time course to the changes in long-range synchronization we report here (Figure 3).

Other brain structures involved in abrupt learning

The most dramatic form of abrupt learning is one-shot learning, in which only a single instance of a stimulus is provided.[65] This kind of learning is closely related to episodic memory, which depends critically on the hippocampus.[66] Interactions between PFC and hippocampus have been shown to correlate with learning on short timescales in monkeys[28] and rodents.[67] In humans, the hippocampus is recruited by PFC when one-shot learning is dictated by the demands of a task.[68] Thus, it might be that PFC establishes the conditions for learning, but that information is initially stored in the hippocampus[69] and then later consolidated into long-term memory.[70]

For tasks that involve a saccadic response, neurons in the caudate nucleus facilitate saccades toward rewarded locations and these signals can update rapidly as contingencies change.[56,71] Indeed, Williams and Eskandar found that firing rates in the caudate correlate with the rate of learning in a task that requires learning to saccade to a particular visual stimulus.[72] The output of these neurons could therefore be linked to the synchronization changes we have observed (Figure 4), which also correlate with the rate of learning.

This connection between dopaminergic cells and learning in PFC has been studied by Puig and Miller, who showed that dopaminergic drugs in PFC can modulate associative learning.[50] Specifically, the antagonists of some dopamine receptors block the formation of new associations, but they do not impair the recall of those already established. Putting these results together, it could be that dopamine released from the caudate facilitates the formation of new or stronger connections between informative sites in IT and longer-term storage in the hippocampus, with PFC playing a permissive role in "switching on" rapid learning.[52,73] Previous work has also highlighted a role for the amygdala in this process.[22,74]

Rapid learning has also been found in auditory tasks.[75] For example, observers exposed to meaningless sounds learn to recognize them after repeated exposures—as in our foraging task, this kind of learning occurs abruptly and endures for several weeks afterward.[76] Learning in both types of tasks might reflect a general mechanism for assimilating statistical regularities about the environment.[77]

Alternative interpretations

In addition to providing signals about reward outcomes, PFC plays a role in arousal, working memory, and attention,[35] all of which are important for learning.[1] Though it is notoriously difficult to disentangle these factors,[78] we have shown several lines of evidence suggesting that none of them alone are sufficient to explain our findings. First, non-specific effects like arousal would not account for the preference for informative IT electrodes in the synchronization between IT and PFC (Figure 4). Thus, while we favor the interpretation of a non-specific signal emanating from PFC (Figure 5), we suggest that it is more parsimonious to think of it as carrying information about reward, rather than arousal per se.[34] Second, working memory might account for the retention of visual associations within each testing session, and it has been often associated with both gamma[79] and alpha synchronization.[80,81] However, by itself it cannot account for the animals' ability to remember the associations many days later.

This long-term recall also supports the idea that changes in behavioral performance in our foraging task reflect genuine visual learning. This is in contrast to an alternative possibility, namely that the data reflect a shift in behavioral strategy between early and later trials. Such shifts might be expected to alter the dynamics of prefrontal activity[82] but it is not clear why they would lead to the pattern of synchronization changes we have observed (Figure 3), why this pattern would emphasize the informative IT electrodes (Figure 4), or why it would have effects that persisted many weeks later.

Finally, we have not specifically controlled top-down attention in this task, as part of our goal was to simulate learning under natural conditions. Attention could therefore have played various roles in learning or overall task performance.[83] Of these roles, the most commonly observed consequence of attention is an improvement in sensory coding, which we did not observe in our data (Figure 7). However, our data are consistent with a different role for attention, namely that of selecting relevant visual inputs based on reward.[83,84] As mentioned above, such a role is consistent with both the gamma synchronization we observe[85] and its specificity for informative sensory signals (Figure 4). Previous work has found that this kind of attentional mechanism is especially important for extracting relevant information from complex stimuli[86,87] of the kind we have used in our foraging task, and so it could have been a factor in our data as well.

STAR★METHODS

Detailed methods are provided in the online version of this paper and include the following:

- KEY RESOURCES TABLE
- RESOURCE AVAILABILITY
  - Lead contact
  - Materials availability
  - Data and code availability
- EXPERIMENTAL MODEL AND SUBJECT DETAILS
  - Animals
- METHOD DETAILS
  - Implant preparation and surgical procedures
  - Behavioral task
  - Eye calibration
  - Saccadic eye movements
  - Processing of raw neural data
  - Trial epoch selection
  - Calculation of spectral power
  - Synchronization
  - Calculation of spectral Granger-Geweke causality
  - Multi-unit analysis
- QUANTIFICATION AND STATISTICAL ANALYSIS
  - Response modeling
  - Statistics

SUPPLEMENTAL INFORMATION

Supplemental information can be found online at https://doi.org/10.1016/j.cub.2022.04.029.

ACKNOWLEDGMENTS

This work was funded by a grant from the CIHR to C.C.P. (PJT-461642) and a graduate student fellowship to B.A.C. from NSERC. We thank Dr. Shahab Bakhtiari and Tugce Gurbuz for the helpful comments and discussions.

AUTHOR CONTRIBUTIONS

M.R.K. and C.C.P. designed the study. M.R.K. and T.P.Z. performed the experiments. B.A.C. analyzed the data. B.A.C., M.R.K., and C.C.P. wrote the paper.

DECLARATION OF INTERESTS

The authors declare no competing interests.

Received: November 24, 2021
Revised: March 8, 2022
Accepted: April 12, 2022
Published: May 5, 2022

REFERENCES

1. Watanabe, T., and Sasaki, Y. (2015). Perceptual learning: toward a comprehensive theory. Annu. Rev. Psychol. *66*, 197–221.
2. Laamerad, P., Guitton, D., and Pack, C.C. (2020). Eye movements shape visual learning. Proc. Natl. Acad. Sci. USA *117*, 8203–8211.
3. Reingold, E.M., and Sheridan, H. (2011). Eye movements and visual expertise in chess and medicine. In The Oxford Handbook of Eye Movements, S.P. Liversedge, I.D. Gilchrist, and S. Everling, eds. (Oxford University Press), pp. 523–550.
4. Ghose, G.M., and Maunsell, J.H.R. (2002). Attentional modulation in visual cortex depends on task timing. Nature *419*, 616–620.
5. Schoups, A., Vogels, R., Qian, N., and Orban, G. (2001). Practising orientation identification improves orientation coding in V1 neurons. Nature *412*, 549–553.
6. Rubin, N., Nakayama, K., and Shapley, R. (1997). Abrupt learning and retinal size specificity in illusory-contour perception. Curr. Biol. *7*, 461–467.
7. Ahissar, M., and Hochstein, S. (1997). Task difficulty and the specificity of perceptual learning. Nature *387*, 401–406.
8. Standing, L. (1973). Learning 10000 pictures. Q. J. Exp. Psychol. *25*, 207–222.
9. Hebb, D.O. (1949). The Organization of Behavior: a Neuropsychological Theory (Wiley).
10. Brea, J., and Gerstner, W. (2016). Does computational neuroscience need new synaptic learning paradigms? Curr. Opin. Behav. Sci. *11*, 61–66.
11. Verbeke, P., and Verguts, T. (2019). Learning to synchronize: how biological agents can couple neural task modules for dealing with the stability-plasticity dilemma. PLoS Comput. Biol. *15*, e1006604.
12. Masse, N.Y., Grant, G.D., and Freedman, D.J. (2018). Alleviating catastrophic forgetting using context-dependent gating and synaptic stabilization. Proc. Natl. Acad. Sci. USA *115*, E10467–E10475.
13. Jutras, M.J., Fries, P., and Buffalo, E.A. (2009). Gamma-band synchronization in the macaque hippocampus and memory formation. J. Neurosci. *29*, 12521–12531.
14. Fell, J., and Axmacher, N. (2011). The role of phase synchronization in memory processes. Nat. Rev. Neurosci. *12*, 105–118.
15. Sauseng, P., Klimesch, W., Doppelmayr, M., Pecherstorfer, T., Freunberger, R., and Hanslmayr, S. (2005). EEG alpha synchronization and functional coupling during top-down processing in a working memory task. Hum. Brain Mapp. *26*, 148–155.
16. Fries, P. (2015). Rhythms for cognition: communication through coherence. Neuron *88*, 220–235.
17. Freedman, D.J., Riesenhuber, M., Poggio, T., and Miller, E.K. (2001). Categorical representation of visual stimuli in the primate prefrontal cortex. Science *291*, 312–316.
18. Kar, K., and DiCarlo, J.J. (2021). Fast recurrent processing via ventrolateral prefrontal cortex is needed by the priamte ventral stream for robus core visual object recognition. Neuron *109*, 164–176.e165.
19. Browning, P.G., Easton, A., Buckley, M.J., and Gaffan, D. (2005). The role of prefrontal cortex in object-in-place learning in monkeys. Eur. J. Neurosci. *22*, 3281–3291.
20. Chukoskie, L., Snider, J., Mozer, M.C., Krauzlis, R.J., and Sejnowski, T.J. (2013). Learning where to look for a hidden target. Proc. Natl. Acad. Sci. USA *110*, 10438–10445.
21. Krause, M.R., Zanos, T.P., Csorba, B.A., Pilly, P.K., Choe, J., Phillips, M.E., Datta, A., and Pack, C.C. (2017). Transcranial direct current stimulation facilitates associative learning and alters functional connectivity in the primate brain. Curr. Biol. *27*, 3086–3096.e3.
22. Ludmer, R., Dudai, Y., and Rubin, N. (2011). Uncovering camouflage: amygdala activation predicts long-term memory of induced perceptual learning. Neuron *69*, 1002–1014.
23. Menzel, C.R. (1991). Cognitive aspects of foraging in Japanese monkeys. Anim. Behav. *41*, 397–402.
24. Tanaka, K. (1996). Inferotemporal cortex and object vision. Annu. Rev. Neurosci. *19*, 109–139.
25. Asaad, W.F., Rainer, G., and Miller, E.K. (1998). Neural activity in the primate prefrontal cortex during associative learning. Neuron *21*, 1399–1407.
26. Hasegawa, I., Hayashi, T., and Miyashita, Y. (1999). Memory retrieval under the control of the prefrontal cortex. Ann. Med. *31*, 380–387.

27. Kornblith, S., and Tsao, D.Y. (2017). How thoughts arise from sights: inferotemporal and prefrontal contributions to vision. Curr. Opin. Neurobiol. *46*, 208–218.

28. Brincat, S.L., and Miller, E.K. (2015). Frequency-specific hippocampal-prefrontal interactions during associative learning. Nat. Neurosci. *18*, 576–581.

29. Pesaran, B., Hagan, M., Qiao, S., and Shewcraft, R. (2021). Multiregional communication and the channel modulation hypothesis. Curr. Opin. Neurobiol. *66*, 250–257.

30. Majaj, N.J., Hong, H., Solomon, E.A., and DiCarlo, J.J. (2015). Simple learned weighted sums of inferior temporal neuronal firing rates accurately predict human core object recognition performance. J. Neurosci. *35*, 13402–13418.

31. Rajalingham, R., and Dicarlo, J.J. (2019). Reversible inactivation of different millimeter-scale regions of primate IT results in different patterns of core object recognition deficits. Neuron *102*, 493–505.e5.

32. O'Scalaidhe, S.P.O., Wilson, F.A.W., and Goldman-Rakic, P.S. (1999). Face-selective neurons during passive viewing and working memory performance of rhesus monkeys: evidence for intrinsic specialization of neuronal coding. Cereb. Cortex *9*, 459–475.

33. Kobayashi, S., Kawagoe, R., Takikawa, Y., Koizumi, M., Sakagami, M., and Hikosaka, O. (2007). Functional differences between macaque prefrontal cortex and caudate nucleus during eye movements with and without reward. Exp. Brain Res. *176*, 341–355.

34. Roelfsema, P.R., and van Ooyen, A. (2005). Attention-gated reinforcement learning of internal representations for classification. Neural Comput. *17*, 2176–2214.

35. Sakagami, M., and Pan, X. (2007). Functional role of the ventrolateral prefrontal cortex in decision making. Curr. Opin. Neurobiol. *17*, 228–233.

36. Kobatake, E., Wang, G., and Tanaka, K. (1998). Effects of shape-discrimination training on the selectivity of inferotemporal cells in adult monkeys. J. Neurophysiol. *80*, 324–330.

37. Li, N., and DiCarlo, J.J. (2010). Unsupervised natural visual experience rapidly reshapes size-invariant object representation in inferior temporal cortex. Neuron *67*, 1062–1075.

38. Brincat, S.L., and Miller, E.K. (2016). Prefrontal cortex networks shift from external to internal modes during learning. J. Neurosci. *36*, 9739–9754.

39. Mukai, I., Kim, D., Fukunaga, M., Japee, S., Marrett, S., and Ungerleider, L.G. (2007). Activations in visual and attention-related areas predict and correlate with the degree of perceptual learning. J. Neurosci. *27*, 11401–11411.

40. Liu, L.D., and Pack, C.C. (2017). The contribution of area MT to visual motion perception depends on training. Neuron *95*, 436–446.e3.

41. Eldridge, M.A.G., Hines, B.E., and Murray, E.A. (2021). The visual prefrontal cortex and anthropoids: interaction with temporal cortex in decision making and its role in the making of 'visual animals'. Curr. Opin. Behav. Sci. *41*, 22–29.

42. Rubin, N., Nakayama, K., and Shapley, R. (2002). The role of insight in perceptual learning: evidence from illusory contour perception. In Perceptual Learning, M. Fahle, and T. Poggio, eds. (MIT Press), pp. 235–251.

43. Jacobs, R.A. (2009). Adaptive precision pooling of model neuron activities predicts the efficiency of human visual learning. J. Vis. *9*, 22. 1–22.15.

44. Bakhtiari, S., Awada, A., and Pack, C.C. (2020). Influence of stimulus complexity on the specificity of visual perceptual learning. J. Vis. *20*, 1–19.

45. Law, C.T., and Gold, J.I. (2010). Shared mechanisms of perceptual learning and decision making. Top. Cogn. Sci. *2*, 226–238.

46. Roelfsema, P.R., van Ooyen, A., and Watanabe, T. (2010). Perceptual learning rules based on reinforcers and attention. Trends Cogn. Sci. *14*, 64–71.

47. Miltner, W.H.R., Braun, C., Arnold, M., Witte, H., and Taub, E. (1999). Coherene of gamma-band EEG activity as a basis for associative learning. Nature *397*, 434–436.

48. Verbeke, P., Ergo, K., De Loof, E., and Verguts, T. (2021). Learning to synchronize: midfrontal theta dynamics during rule switching. J. Neurosci. *41*, 1516–1528.

49. Santarnecchi, E., Sprugnoli, G., Bricolo, E., Costantini, G., Liew, S.-L., Musaeus, C.S., Salvi, C., Pascual-Leone, A., Rossi, A., and Rossi, S. (2019). Gamma tACS over the temporal lobe increases the occurrence of Eureka! moments. Sci. Rep. *9*, 5778.

50. Puig, M.V., and Miller, E.K. (2012). The role of prefrontal dopamine D1 receptors in the neural mechanisms of associative learning. Neuron *74*, 874–886.

51. Jensen, O., Gelfand, J., Kounios, J., and Lisman, J.E. (2002). Oscillations in the alpha band (9–12 Hz) increase with memory load during retention in a short-term memory task. Cereb. Cortex *12*, 877–882.

52. Miller, E.K., and Cohen, J.D. (2001). An integrative theory of prefrontal cortex function. Annu. Rev. Neurosci. *24*, 167–202.

53. Meyers, E.M., Qi, X.-L., and Constantinidis, C. (2012). Incorporation of new information into prefrontal cortical activity after learning working memory tasks. Proc. Natl. Acad. Sci. USA *109*, 4651–4656.

54. Durstewitz, D., Vittoz, N.M., Floresco, S.B., and Seamans, J.K. (2010). Abrupt transitions between prefrontal neural ensemble states accompany behavioral transitions during rule learning. Neuron *66*, 438–448.

55. Cromer, J.A., Machon, M., and Miller, E.K. (2011). Rapid association learning in the primate prefrontal cortex in the absence of behavioral reversals. J. Cogn. Neurosci. *23*, 1823–1828.

56. Pasupathy, A., and Miller, E.K. (2005). Different time courses of learning-related activity in the prefrontal cortex and striatum. Nature *433*, 873–876.

57. Asaad, W.F., Lauro, P.M., Perge, J.A., and Eskandar, E.N. (2017). Prefrontal neurons encode a solution to the credit-assignment problem. J. Neurosci. *37*, 6995–7007.

58. Tovee, M.J., Rolls, E.T., and Ramachandran, V.S. (1996). Rapid visual learning in neurones of the prime temporal visual cortex. NeuroReport *7*, 2757–2760.

59. Khan, A.G., Poort, J., Chadwick, A., Blot, A., Sahani, M., Mrsic-Flogel, T.D., and Hofer, S.B. (2018). Distinct learning-induced changes in stimulus selectivity and interactions of GABAergic interneuron classes in visual cortex. Nat. Neurosci. *21*, 851–859.

60. Logothetis, N., Pauls, J., and Poggio, T. (1995). Spatial Reference Frames for Object Recognition. Tuning for Rotations In Depth (MIT Artificial Intelligence Laboratory, MIT School of Science, Center for Biological & Computational Learning).

61. Adab, H.Z., Popivanov, I.D., Vanduffel, W., and Vogels, R. (2014). Perceptual learning of simple stimuli modifies stimulus representations in posterior inferior temporal cortex. J. Cogn. Neurosci. *26*, 2187–2200.

62. Yang, T., and Maunsell, J.H.R. (2004). The effect of perceptual learning on neuronal response in monkey visual area V4. J. Neurosci. *24*, 1617–1626.

63. Adab, H.Z., and Vogels, R. (2011). Practicing coarse orientation discrimination improves orientation signals in Macaque cortical area V4. Curr. Biol. *21*, 1661–1666.

64. Wang, Y., and Dragoi, V. (2015). Rapid learning in visual cortical networks. eLife *4*, e08417.

65. Cook, R., and Fagot, J. (2009). First trial rewards promote 1-trial learning and prolonged memory in pigeon and baboon. Proc. Natl. Acad. Sci. USA *106*, 9530–9533.

66. Eichenbaum, H. (2000). A cortical-hippocampal system for declarative memory. Nat. Rev. Neurosci. *1*, 41–50.

67. Benchenane, K., Peyrache, A., Khamassi, M., Tierney, P.L., Gioanni, Y., Battaglia, F.P., and Wiener, S.I. (2010). Coherent theta oscillations and reorganization of spike timing in the hippocampal-prefrontal network upon learning. Neuron *66*, 921–936.

68. Lee, S.W., O'Doherty, J.P., and Shimojo, S. (2015). Neural computations mediating one-shot learning in the human brain. PLoS Biol. *13*, e1002137.

69. McClelland, J.L., McNaughton, B.L., and O'Reilly, R.C. (1995). Why there are complementary learning systems in the hippocampus and neocortex: insights from the successes and failures of connectionist models of learning and memory. Psychol. Rev. *102*, 419–457.

70. Tse, D., Langston, R.F., Kakeyama, M., Bethus, I., Spooner, P.A., Wood, E.R., Witter, M.P., and Morris, R.G.M. (2007). Schemas and memory consolidation. Science *316*, 76–82.

71. Watanabe, K., and Hikosaka, O. (2005). Immediate changes in anticipatory activity of caudate neurons associated with reversal of position-reward contigency. J. Neurophysiol. *94*, 1879–1887.

72. Williams, Z.M., and Eskandar, E.N. (2006). Selective enhancement of associative learning by microstimulation of the anterior caudate. Nat. Neurosci. *9*, 562–568.

73. Petrov, A.A., Dosher, B.A., and Lu, Z.-L. (2005). The dynamics of perceptual learning: an incremental re-weighting model. Psychol. Rev. *112*, 715–743.

74. Paton, J.J., Belova, M.A., Morrison, S.E., and Salzman, C.D. (2006). The primate amygdala represents the positive and negative value of visual stimuli during learning. Nature *439*, 865–870.

75. Seitz, A.R. (2010). Sensory learning: rapid extraction of meaning from noise. Curr. Biol. *20*, R643–R644.

76. Agus, T.R., Thorpe, S.J., and Pressnitzer, D. (2010). Rapid formation of robust auditory memories: insights from noise. Neuron *66*, 610–618.

77. Chun, M.M. (2000). Contextual cueing of visual attention. Trends Cogn. Sci. *4*, 170–178.

78. Maunsell, J.H.R. (2004). Neuronal representations of cognitive state: reward or attention? Trends Cogn. Sci. *8*, 261–265.

79. Salazar, R.F., Dotson, N.M., Bressler, S.L., and Gray, C.M. (2012). Content-specific fronto-parietal synchronization during visual working memory. Science *338*, 1097–1100.

80. Palva, S., and Palva, J.M. (2011). Functional roles of alpha-band phase synchronization in local and large-scale cortical networks. Front. Psychol. *2*, 204.

81. Neupane, S., Guitton, D., and Pack, C.C. (2017). Coherent alpha oscillations link current and future receptive fields during saccades. Proc. Natl. Acad. Sci. USA *114*, E5979–E5985.

82. Ebitz, B.R., Albarran, E., and Moore, T. (2018). Exploration disrupts choice-predictive signals and alters dynamics in prefrontal cortex. Neuron *97*, 450–461.e9.

83. Serences, J.T., and Kastner, S. (2014). A multi-level account of selective attention. In The Oxford Handbook of Attention, A.C. Nobre, and S. Kastner, eds. (Oxford University Press), pp. 76–104.

84. Baruni, J.K., Lau, B., and Salzman, C.D. (2015). Reward expectation differentially modulates attentional behavior and activity in visual area V4. Nat. Neurosci. *18*, 1656–1663.

85. Gregoriou, G.G., Gotts, S.J., Zhou, H., and Desimone, R. (2009). High-frequency, long-range coupling between prefrontal and visual cortex during attention. Science *324*, 1207–1210.

86. Pestilli, F., Carrasco, M., Heeger, D.J., and Gardner, J.L. (2011). Attentional enhancement via selection and pooling of early sensory responses in human visual cortex. Neuron *72*, 832–846.

87. Niv, Y., Daniel, R., Geana, A., Gershman, S.J., Leong, Y.C., Radulescu, A., and Wilson, R.C. (2015). Reinforcement learning in multi-dimensional environments relies on attention mechanisms. J. Neurosci. *35*, 8145–8157.

88. Mitra, P., and Bokil, H. (2008). Observed Brain Dynamics (Oxford University Press).

89. Otero-Millan, J., Alba Castro, J.L., Macknik, S.L., and Martinez-Conde, S. (2014). Unsupervised clustering method to detect microsaccades. J. Vis. *14*, 1–17.

90. Fedorov, A., Beichel, R., Kalpathy-Cramer, J., Finet, J., Fillion-Robin, J.C., Pujol, S., Bauer, C., Jennings, D., Fennessy, F., Sonka, M., et al. (2012). 3D Slicer as an image computing platform for the quantitative imaging network. Magn. Reson. Imaging *30*, 1323–1341.

91. Markov, N.T., Ercsey-Ravasz, M.M., Ribeiro Gomes, A.R., Lamy, C., Magrou, L., Vezoli, J., Misery, P., Falchier, A., Quilodran, R., Gariel, M.A., et al. (2014). A weighted and directed interareal connectivity matrix for macaque cerebral cortex. Cereb. Cortex *24*, 17–36.

92. Cornelissen, F.W., Peters, E.M., and Palmer, J. (2002). The eyelink toolbox: eye tracking with MATLAB and the psychophysics toolbox. Behav. Res. Methods Instrum. Comput. *34*, 613–617.

93. Zanos, T.P., Mineault, P.J., Nasiotis, K.T., Guitton, D., and Pack, C.C. (2015). A sensorimotor role for traveling waves in primate visual cortex. Neuron *85*, 615–627.

94. Jutras, M.J., Fries, P., and Buffalo, E.A. (2013). Oscillatory activity in the monkey hippocampus during visual exploration and memory formation. Proc. Natl. Acad. Sci. USA *110*, 13144–13149.

95. Pesaran, B. (2008). Spectral analysis for neural signals. In Neural Signal Processing: Quantitative Analysis of Neural Activity, P. Mitra, ed. (Society for Neuroscience), pp. 1–12.

96. Zeitler, M., Fries, P., and Gielen, S. (2006). Assessing neuronal coherence with single-unit, multi-unit and local field potentials. Neural Comput. *18*, 2256–2281.

97. Harris, A.Z., and Gordon, J.A. (2015). Long-range neural synchrony in behavior. Annu. Rev. Neurosci. *38*, 171–194.

98. Dhamala, M., Liang, H., Bressler, S.L., and Ding, M. (2018). Granger-Geweke causality: estimation and interpretration. NeuroImage *175*, 460–463.

99. Corain, L., and Salmaso, L. (2007). A critical review and a comparative study on conditional permutation tests for two-way ANOVA. Commun. Stat. Simul. Comput. *36*, 791–805.

100. Benjamini, Y., and Yekutieli, D. (2005). False discovery rate—adjusteed multiple confidence intervals for selected parameters. J. Am. Stat. Assoc. *100*, 71–81.

STAR★METHODS

KEY RESOURCES TABLE

REAGENT or RESOURCE	SOURCE	IDENTIFIER
Experimental models: Organisms/strains		
Rhesus macaque, Macaca mulatta (males, 4 and 10 years)	McGill University	N/A
Software and algorithms		
MATLAB R2016b	Mathworks	RRID: SCR_001622
Chronux	http://chronux.org [88]	v2.12.3
Microsaccade Detection	Otero-Millan et al.[89]	N/A
3D Slicer	https://slicer.org [90]	4.11
Custom code	This paper	https://github.com/bennettcsorba/AbruptLearning
Other		
Utah multielectrode arrays	Blackrock Microsystems, Utah (USA)	Iridium Oxide, 96 Channel
Macaque Atlas (Figure 2)	Markov et al.[91]	Core-Nets https://core-nets.org

RESOURCE AVAILABILITY

Lead contact

Requests for information or resources should be directed to the lead contact, Bennett Csorba (bennett.csorba@mail.mcgill.ca).

Materials availability

This study did not generate any unique materials.

Data and code availability

- All behavioral and neural data used in this study are available from the lead contact upon request (due to the size of the data set).
- All custom MATLAB scripts related to this paper are available on GitHub (https://github.com/bennettcsorba/AbruptLearning) and are publicly available as of the date of publication.
- Any additional information required to reanalyze the data reported in this paper is available from the lead contact upon request.

EXPERIMENTAL MODEL AND SUBJECT DETAILS

Animals

Two adult male rhesus macaque monkeys (*Macaca mulatta*, 4 and 10 years old) participated in the study. All animal care, surgical and experimental procedures were approved by the Montreal Neurological Institute's Animal Care Committee, and the animals were monitored by the veterinary staff for the duration of the experiment.

METHOD DETAILS

In some experiments on the same animals, we examined the influence of transcranial direct current stimulation (tDCS) on neural activity and behavior. These data have been reported in a separate paper[21] and were excluded from the analyses reported here.

Implant preparation and surgical procedures

Experimental preparation has been described in a previous publication.[21] In brief, high-resolution T1 and T2-weighted anatomical MRIs (0.6-0.8 mm^3 voxels) were acquired for each animal and were used for surgical planning. Animals were implanted with a custom titanium head post (Hybex Innovations, Montreal Canada) using standard sterile surgical techniques. Post-recovery, animals were

familiarized with the laboratory environment, and were trained for head fixation and subsequently the behavioral ''foraging'' task. Once overall performance in this paradigm was stable, we prepared the animals for electrophysiology.

A second surgery was then performed to implant multielectrode arrays (Blackrock Microsystems; Utah, USA) into IT (area TEO) and the lateral PFC, ventral to the principal sulcus (area 46v). This part of PFC receives projections from IT and is often considered part of the machinery for visual image recognition. A neuro-navigation system (Brainsight Vet; Rogue Research Montreal Canada) synced with previously completed MRI scans[90] was used to ensure that the arrays were accurately positioned. Arrays were then inserted into PFC and IT using a pneumatic device. The positions of the arrays were verified post-operatively (Figure 2), via coregistration of pre-operative MRI scans with postoperative CT scans.

Behavioral task

Non-human primates were seated in front of a screen that spanned 30x60 degrees of visual angle, at a viewing distance of 40 cm. Eye positions were sampled at 500 Hz with an infrared eye tracker (SR Research, Ontario). During each session, the animals completed the foraging task described below over the course of approximately 30 minutes, with each trial following the progression shown in Figure 1A. Foraging trials were alternated with brief trials involving a calibration task (see below), to ensure precise calibration of the eye tracker. The foraging paradigm was adapted from a previous study which investigated associative learning in humans.[20]

Each trial of the foraging task began with the appearance of a high-contrast fixation cross on a gray screen. Animals initiated the trial by fixating within 2 degrees of the fixation spot for 750–1000 ms, after which they were presented with a full-screen image. Images were chosen from collections of Creative-Commons and public domain photographs of natural images (url: flickr.com). Image presentation order was randomized within each session, and sessions consisted of 75 or 100 trials (depending on the animal) of each of the two images.

A 2^{o} reward zone (RZ) was embedded into a random location in each image, and jittered a small amount on each trial, according to a bivariate normal distribution with a standard deviation of 1–4 degrees. This encouraged the subjects to learn the spatiotopic location of the RZ, rather than a specific set of saccade vectors (Figures S1G–S1J), as the RZ was positioned differently relative to the starting eye position on each trial (Figures S1K and S1L). Upon image presentation, animals could freely search the image until they found the RZ or 15 (Monkey F) or 20 (Monkey M) seconds elapsed. If animals did not successfully find the RZ within that time, a high-contrast cue was shown at the RZ to guide their saccades into it. Once the animals had successfully maintained gaze position within the RZ for 100 ms, they received a juice reward and the trial ended.

Throughout our electrophysiological recordings, behavioral performance was not associated with session number (linear regression between session number and N_{50}, $R^2 = 0.04$, $p = 0.12$), as animals were trained extensively on the task prior to the commencement of neural recordings. Thus, any fluctuations in performance across sessions are likely due to differences in image difficulty or engagement.

In the main experiment, images were not repeated across sessions. We also conducted 19 long-term recall sessions, in which animals ''foraged'' in image-reward zone pairs that they had seen 3–128 days earlier. Behavioral performance during these sessions is described separately in the Results, but the data are not included in any of the electrophysiological analyses.

Eye calibration

Eye calibration was checked on interleaved trials in which the animals were shown a grey screen with a single small, high-contrast saccade target, randomly located at one of 9 (or 25) locations on a 3x3 (or 5x5) grid spanning the central 14 horizontal and vertical degrees on the monitor (Figure S7I). Animals received a liquid reward for making a saccade to the target and maintaining their gaze on it for 750–1,250 ms.

Saccadic eye movements

Saccade onset and offset were estimated from the eye position traces based on eye velocity and acceleration,[92] followed by manual review to make small corrections to onset/offset times and to discard false detections. Microsaccades were extracted using an unsupervised clustering method.[89]

Processing of raw neural data

Wideband neural signals were recorded using a neural interface processor (Ripple Neuro, Salt Lake City, Utah). Neural signals were sampled at 30,000 Hz and band-pass filtered between 0.3 and 7,500 Hz during acquisition. These data were post-processed offline to remove powerline and low-frequency movement artifacts, using the Chronux[88] functions `rmlinesc` and `locdetrend` respectively. Next, the local field potentials (LFPs) were extracted with a fourth order Butterworth low-pass filter (F_c = 500 Hz) and resampled at 1 kHz.

Subsequent analysis was performed with the MATLAB signal processing package Chronux (v2.12.3) and custom-written MATLAB software. The LFPs were manually reviewed for quality. Sites were excluded from analysis on individual sessions when they had an exceptionally low signal-to-noise ratio (SNR < 3). An average of 89 out of 96 IT sites, (*SE*=0.33, > 92% of all sites) and 95 of 96 PFC sites (*SE*=0.12, > 98% of all sites) were available for analysis.

Trial epoch selection

Three epochs of interest (Figure 1A) were chosen from the data from each trial: a Scene Onset epoch (400ms following scene onset), a Reward epoch (400ms following reward onset), and a Foraging epoch (225ms to 100ms before the onset of the first saccade on each trial). We chose to limit the analysis of the Foraging epoch to the time just before the onset of the first saccade because the free-viewing paradigm rendered the Foraging epoch otherwise uncontrolled in terms of eye movements and visual stimulation. In particular, eye movements can strongly influence LFP signals.[93,94]

The epoch durations were chosen based on preliminary analyses (Figure 3), with the intention to identify regions of interest in time-frequency space. Other bands and window sizes around these event epochs were considered for all reported neurophysiological measures to avoid biasing the results. See Figures 3 and S3; Figure S4 for other frequency bands, which showed no effect.

Calculation of spectral power

Within each epoch, we estimated the LFP power with multi-taper methods, using five tapers and a spectral resolution of 7.5 Hz[95] (Figures S6A and S6B).

For both recording areas, we took the average power across all usable electrodes on each trial, within each trial epoch. For each trial epoch, a maximal trial value was determined, to which all other trial values were normalized. Learning epoch averages were then computed from the normalized values.

Synchronization

To quantify synchronization (Figures 3, 4, 5, 6, S1C, S1D, S2C–S2H, S3, S4, S6C, S6D, and S7A–S7H), we computed LFP-LFP coherence, which is a measure of the linear correlation between two signals in the frequency domain[96,97] and a commonly-used metric of synchronization.[97] Coherence is independent of absolute phase and is often thought of as the consistency across trials of the relative phase angles between two signals. We computed magnitude-squared LFP-LFP coherence with multi-taper methods, using the Chronux[88] functions cohgramc and coherency for continuous signals. Five tapers and a spectral resolution of 7.5 Hz[95] were used. The magnitude-squared coherence between two signals at a given frequency is defined as the cross-power spectrum (also called cross-spectral density) of those two signals divided by their individual power spectra, also taken at that same frequency.

Session averages for LFP-LFP coherence (Figure 4) were computed by taking the median values across usable electrodes within (max. 4,560 pairs each) or between (max. 9,126 pairs) IT and PFC. Because coherence is not defined on a single trial, we used five-trial windows to compute coherence across trials throughout each session. This allowed us to capture relatively abrupt changes in the communication between IT and PFC that occurred over the course of a few trials. The first and last two trials of each session used three-trial and four-trial windows respectively to compute coherence, but these data were rarely used.

As with power, we normalized coherence values to the maximum values within each trial epoch. Normalization was done independently at each frequency. Averages within each learning epoch (Figures 3 and S1C) were then computed from the normalized trial values for each trial epoch.

Correlations between coherence levels and behavior (Figures 3B and 3C) were obtained by subsampling different groups of electrodes in each area 1000 times and computing the linear regression between the time of peak coherence and the N_{50} trial for the corresponding session. Mean values of r^2 ranged from 0.39, for 10 electrodes per area, to 0.73 for 96 electrodes per area. Only the latter value is reported (in Figure 3C).

Calculation of spectral Granger-Geweke causality

Within individual sessions, non-parametric spectral Grange-Geweke causality estimates[98] were computed between all usable electrode pairings, using trial data from three learning epochs for frequency bands of interest. Causal estimates were then averaged by learning epoch across all IT-PFC electrode pairings. The size of the temporal window used in each trial was dependent on the trial epoch (see above).

Multi-unit analysis

Because single-unit activity was generally sparse in both areas, we focused on multi-unit activity in this study (Figure S5). A three-step process was used to extract multi-unit activity from the wideband signals. First, the raw signals were high-pass filtered (F_c = 500 Hz), using a 3rd-order Butterworth filter. Multi-unit events were then defined as the instants where the resulting signal exceeded 3 robustly-estimated standard deviations from the mean (i.e., 4.2 median absolute deviations). To avoid double-counting events, we imposed a 2-ms refractory period immediately after each threshold crossing. We defined MUA responsiveness as the mean rate of MUA events (Figure 7) in units of events/s, occurring on each electrode during the 400 ms after the reward was dispensed (“reward responsiveness”) or after scene onset (“image responsiveness”).

We used a linear discriminant analysis (LDA) to identify subsets of electrodes whose multi-unit activity were more (or less) selective for the scenes being presented, and to determine if neuronal selectivity improved with learning. Classification was done independently for each experimental session, and classifiers were trained separately on IT activity and PFC activity using scene labels as class inputs (Figure 7). Two unique scenes were shown on every session, so the classifier was always trained to discriminate between two data classes. LDA classifiers were trained on multi-unit activity collected on all available electrodes in IT and PFC, using the responses obtained at each site during the scene onset epoch. We chose this epoch because it provided the purest measure of sensory selectivity, without confounding influences of eye movements or rewards.

Classification performance on individual sessions was computed using leave-one-out cross-validation. Because population selectivity did not change post-learning in either IT or PFC (Figure 7A), the classifiers were trained on all trials within a session. Classifiers were also trained on shuffled class data as a control, where the performance was approximately 50%, as expected for a balanced two-way classification task. Classifiers consistently relied on different IT electrodes to classify images across sessions (Figure S2A) in each animal, as would be expected from the variable selectivity of different IT sites.[31]

To determine whether MUAs encoded the location of the RZ, we first identified saccades in the eye calibration trials made to targets located at similar spatial coordinates to the RZ (Figure S7I) and its reflection across both axes. This was done by matching the RZ coordinates for each image to the closest target location (by Euclidean distance) in the calibration task. The median Euclidean distance between the RZ and the closest target location in the calibration task was 2.97 degrees across images. One image whose RZ had both an absolute azimuth and elevation of less than 2 degrees was excluded from this analysis, since the RZ's spatial reflection was directly adjacent to it.

We then used activity recorded during the calibration trials to estimate the response of each MUA signal, during the 250 ms before the onset of the saccade to the corresponding target. From these responses we calculated the preference for the direction of the RZ as a function of the multi-unit firing rates μ:

$$\text{index of selectivity} = \frac{\mu_{similar} - \mu_{opposite}}{\mu_{similar} + \mu_{opposite}}$$

This yielded an index of selectivity, which we used to sort electrodes from most to least selective; we then analyzed interareal coherence levels for different levels of RZ selectivity in each frequency band and epoch (Figure S7). For the retinotopic analysis, the procedure was identical, except that RZs were sorted according to their position relative to the fixation point on each trial. Because the fixation point location varied somewhat from trial to trial (see Foraging task above), the retinotopic and screen coordinate systems were not identical.

To determine whether population activity changed with learning, we generated a vector of population responses for each image, averaging responses across 5 trials. We then correlated the vector with a similar vector calculated from the subsequent 5 trials and repeated this procedure throughout the course of each session.

QUANTIFICATION AND STATISTICAL ANALYSIS

Response modeling

In each session, response times (RTs) for all presentations of each image were extracted. RTs were then smoothed with a three-element median filter to exclude transient lapses in engagement. The resulting response time curves were well-described by sigmoid functions, so the data were fit to a model described by the equation:

$$S(n) = -Gain \times \frac{1}{1 + e^{-Slope + (n - N50)}} + (Gain + MinRT)$$

where $S(n)$ is the response time on the nth presentation of a given image. The *Gain* parameter represents the magnitude of the performance improvement obtained through learning. The parameter *MinRT* reflects the animal's asymptotic performance, or the response time necessary to complete the task once the association had been completely learned.

Similarly, the N_{50} parameter indexes the trial number at which the response time reaches the halfway point between its initial value and its asymptotic value. This parameter therefore identifies the midpoint of the shift from a pre-learning phase to a post-learning phase (Figure 1B). The *Slope* reflects how quickly the response time shifted from its maximum to its minimum.

We excluded data from images in which the parameters of the sigmoid fits were inconsistent with reliable task performance. For example, images for which $N_{50} < 0$ were generally too noisy to be interpreted. Images for which the animal failed to learn the association were those in which N_{50} was greater than 100, *Gain* was less than 3 s, or *MinRT* was greater than 3 s. We verified that the excluded data reflected a lack of learning, in terms of the overall improvement in performance throughout the session, but we did not perform any selection based on the abruptness of learning.

Statistics

To ensure that the results were similar between the two monkeys, we generally used permutative two-way ANOVAs,[99] with monkey identity as a factor. Where appropriate, we used individual t tests. When testing linear correlations between two groups, Pearson's *r* values were computed.

All significance thresholds were corrected for multiple comparisons where necessary. Correcting for multiple comparisons was done by adjusting with a Holm-Bonferroni correction or a false discovery rate criterion,[100] depending on the correct context. All statistical tests were performed in MATLAB.

Current Biology, Volume *32*

Supplemental Information

Long-range cortical synchronization supports abrupt visual learning

Bennett A. Csorba, Matthew R. Krause, Theodoros P. Zanos, and Christopher C. Pack

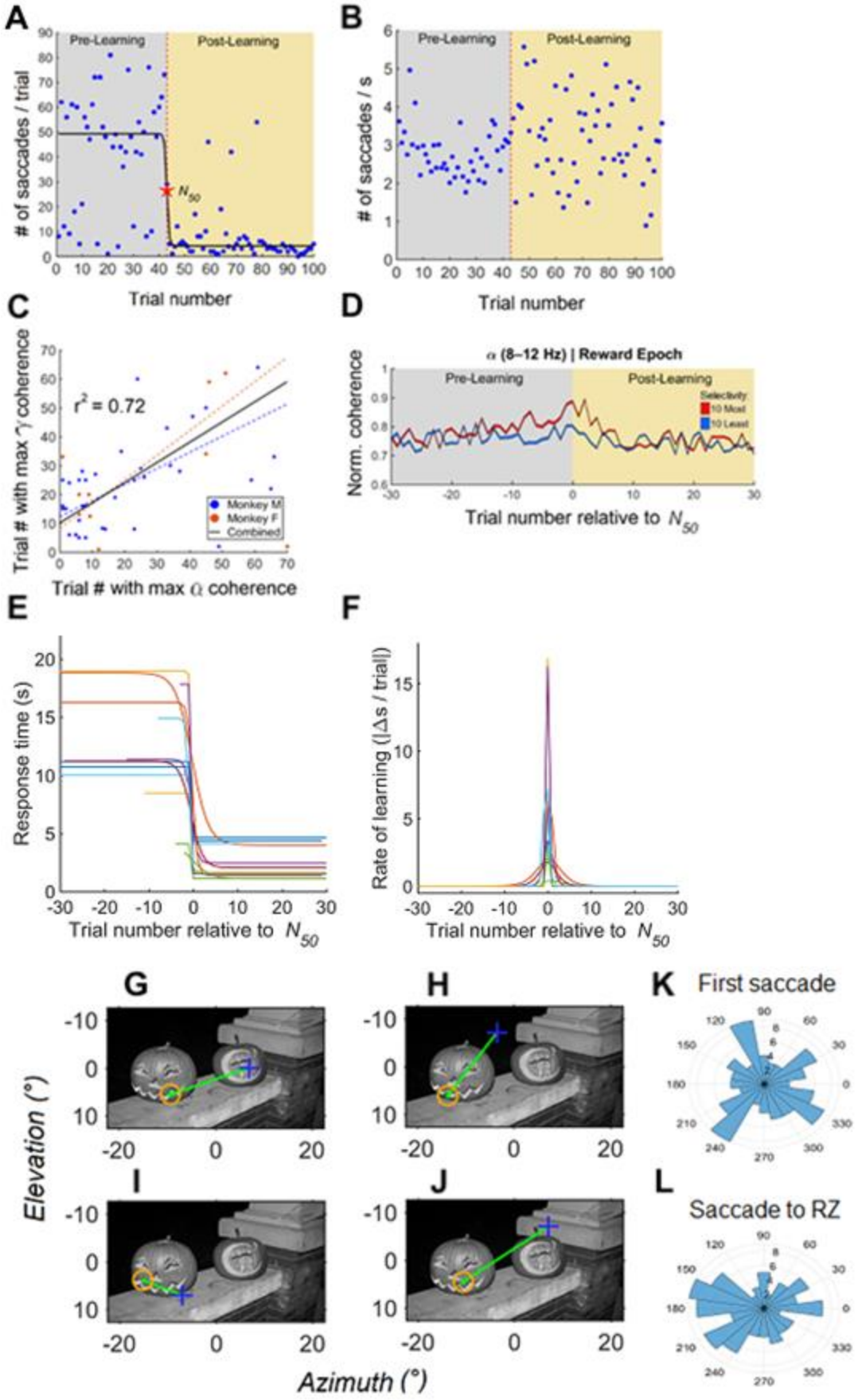
A
Pre-Learning
Post-Learning
# of saccades / trial
N_{50}
Trial number
B
Pre-Learning
Post-Learning
# of saccades / s
Trial number
C
r^2 = 0.72
Monkey M
Monkey F
Combined
Trial # with max γ coherence
Trial # with max α coherence
D
α (8–12 Hz) | Reward Epoch
Pre-Learning
Post-Learning
Selectivity
10 Most
10 Least
Norm. coherence
Trial number relative to N_{50}
E
Response time (s)
Trial number relative to N_{50}
F
Rate of learning (|Δs / trial|)
Trial number relative to N_{50}
G
H
I
J
Elevation (°)
Azimuth (°)
K
First saccade
L
Saccade to RZ

Figure S1. Additional behavioral and neural data for the example session in Figure 1 and split for individual animals. Related to Figure 1 and Figure 4.

(A) The number of saccades made on each trial for the example image from Figure 1 (panel B). The animal transitioned from making many saccades to few saccades to the target around the moment of learning.

(B) The rate at which saccades were made on each trial for the example image in Figure 1 (panel B).

(C) Correlation between trial number with maximum alpha and trial number with maximum gamma coherences.

(D) Synchronization between IT and PFC is shown for the alpha band (8-12 Hz) in the Reward epoch for the example session, with data aligned on the N_{50} trial. The dashed black line represents the grand median of all usable electrode pairs within the session. The red and blue lines correspond to the average strength of synchronization between all PFC sites and those IT sites that are most (red) and least (blue) informative about the images shown in each session. The most informative IT electrodes showed higher alpha synchronization (8-12 Hz) with PFC around the moment of learning in the Reward epoch, as in Figure 4 (panel B). Shading around each line indicates standard error (SEM) across electrodes.

(E) Estimated sigmoid fits for all images for Monkey F, aligned on the N_{50} *value for each image*. Learning is abrupt for most images.

(F) The rate of learning, defined as the performance improvement as a function of trial number, for the images shown in E. Rates are aligned on the N_{50} *value for each image.*

(G-H) Example positions of the starting eye position (blue cross) relative to the RZ (orange circle) for a single image. Trials *before* the image's N_{50} trial.

(I-J) Example positions of the starting eye position (blue cross) relative to the RZ (orange circle) for a single image. Trials *after* the image's N_{50} trial.

(K) For the example image from (G-J), the distribution of directions of the first saccade made on every trial.

(L) For the example image from (G-J), the distribution of directions of the final saccade made (i.e., the saccade to the RZ) on every trial.

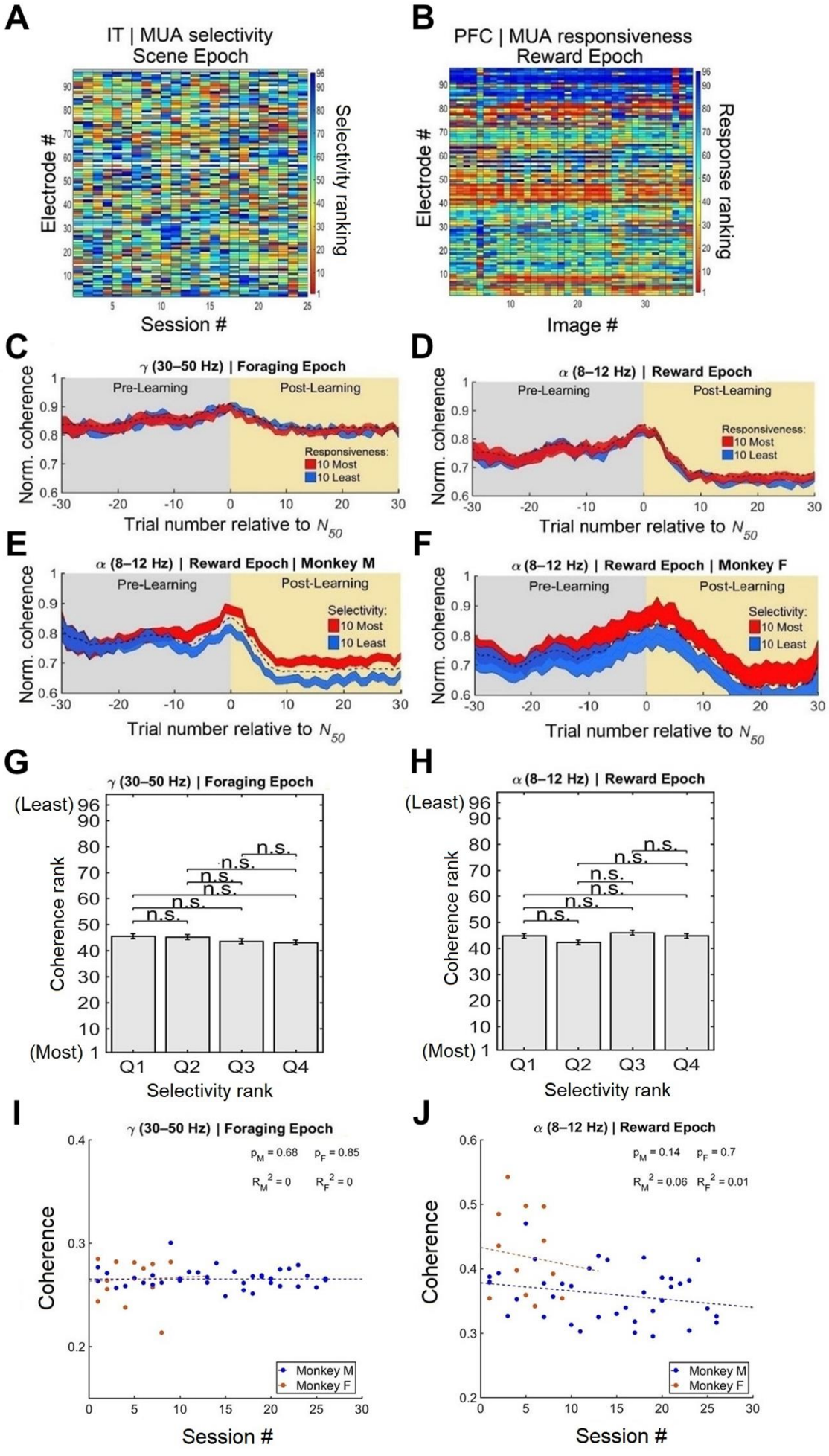
A
IT | MUA selectivity
Scene Epoch
Electrode #
Session #
Selectivity ranking
B
PFC | MUA responsiveness
Reward Epoch
Electrode #
Image #
Response ranking
C
γ (30–50 Hz) | Foraging Epoch
Pre-Learning
Post-Learning
Responsiveness:
10 Most
10 Least
Norm. coherence
Trial number relative to N_{50}
D
α (8–12 Hz) | Reward Epoch
Pre-Learning
Post-Learning
Responsiveness:
10 Most
10 Least
Norm. coherence
Trial number relative to N_{50}
E
α (8–12 Hz) | Reward Epoch | Monkey M
Pre-Learning
Post-Learning
Selectivity:
10 Most
10 Least
Norm. coherence
Trial number relative to N_{50}
F
α (8–12 Hz) | Reward Epoch | Monkey F
Pre-Learning
Post-Learning
Selectivity:
10 Most
10 Least
Norm. coherence
Trial number relative to N_{50}
G
γ (30–50 Hz) | Foraging Epoch
(Least)
(Most)
Coherence rank
n.s.
Q1
Q2
Q3
Q4
Selectivity rank
H
α (8–12 Hz) | Reward Epoch
(Least)
(Most)
Coherence rank
n.s.
Q1
Q2
Q3
Q4
Selectivity rank
I
γ (30–50 Hz) | Foraging Epoch
p_M = 0.68 p_F = 0.85
R_M^2 = 0 R_F^2 = 0
Coherence
Monkey M
Monkey F
Session #
J
α (8–12 Hz) | Reward Epoch
p_M = 0.14 p_F = 0.7
R_M^2 = 0.06 R_F^2 = 0.01
Coherence
Monkey M
Monkey F
Session #

Figure S2. Contribution of different electrodes to image selectivity and reward responses across sessions. IT responsiveness does not drive synchronization. Results are consistent across animals. Related to Figures 4, 5 and 6.

(A) LDA selectivity rankings for every IT site are plotted for each individual session for Monkey M. Red indicates highly informative sites, while blue indicates uninformative sites. The informativeness of each site varies across sessions, indicating that different electrodes were selective for different images.

(B) MUA responsiveness to reward for every PFC site is plotted for each individual session for Monkey M. Red colors indicate highly responsive sites, while blue colors indicate sites with weaker responses. The electrodes that show responses to the reward onset are similar from experiment to experiment.

(C-D) Normalized coherence between IT and PFC is shown low-gamma (30-50 Hz) synchronization during foraging (C) & alpha (8-12 Hz) synchronization following reward (D). Each band represents the grand median of all usable electrode pairs for all images. Error bars display standard error (SEM) across images. Average levels of synchronization, with the data split by *responsiveness* to the appearance of images in IT. For all epochs and bands, there was no statistical difference in the extent to which PFC was synchronized with more responsive (red) and less responsive (blue) sites in IT. The dashed black line indicates the overall average synchronization, which did not change noticeably across trials for these frequencies and these epochs.

(E-F) Figure 4 (panel B) with data for each animal shown separately. The changes in synchronization across time, as well as the preference for informative IT electrodes, are present for each animal individually.

(G-H) Individual sites in IT were sorted based on their average coherence levels with sites in PFC (pre-learning) and checked for differences in decoding accuracy (by quartile) on individual sessions. There was no consistent statistical relationship between coherence levels and decoding accuracy for either the Foraging epoch (using gamma coherence) or the Reward epoch (using alpha coherence) (two-way ANOVAs, $p > 0.05$). Means are of all sites across sessions (Monkey M = 3247 electrodes from 37 images, Monkey F = 1194 electrodes from 13 images), and bars represent standard error (SEM).

(G) Ranking of mean pre-learning low-gamma (30-50 Hz) coherence (Foraging epoch) versus image selectivity rank for IT sites.

(H) Ranking of mean pre-learning alpha (8-12 Hz) coherence (Reward epoch) versus image selectivity rank for IT sites.

(I) Mean alpha (8-12 Hz) non-normalized coherence (early trials) between IT & PFC during the Reward epoch versus session number.

(J) Mean low-gamma (30-50 Hz) non-normalized coherence (early trials) between IT & PFC during the Foraging epoch versus session number.

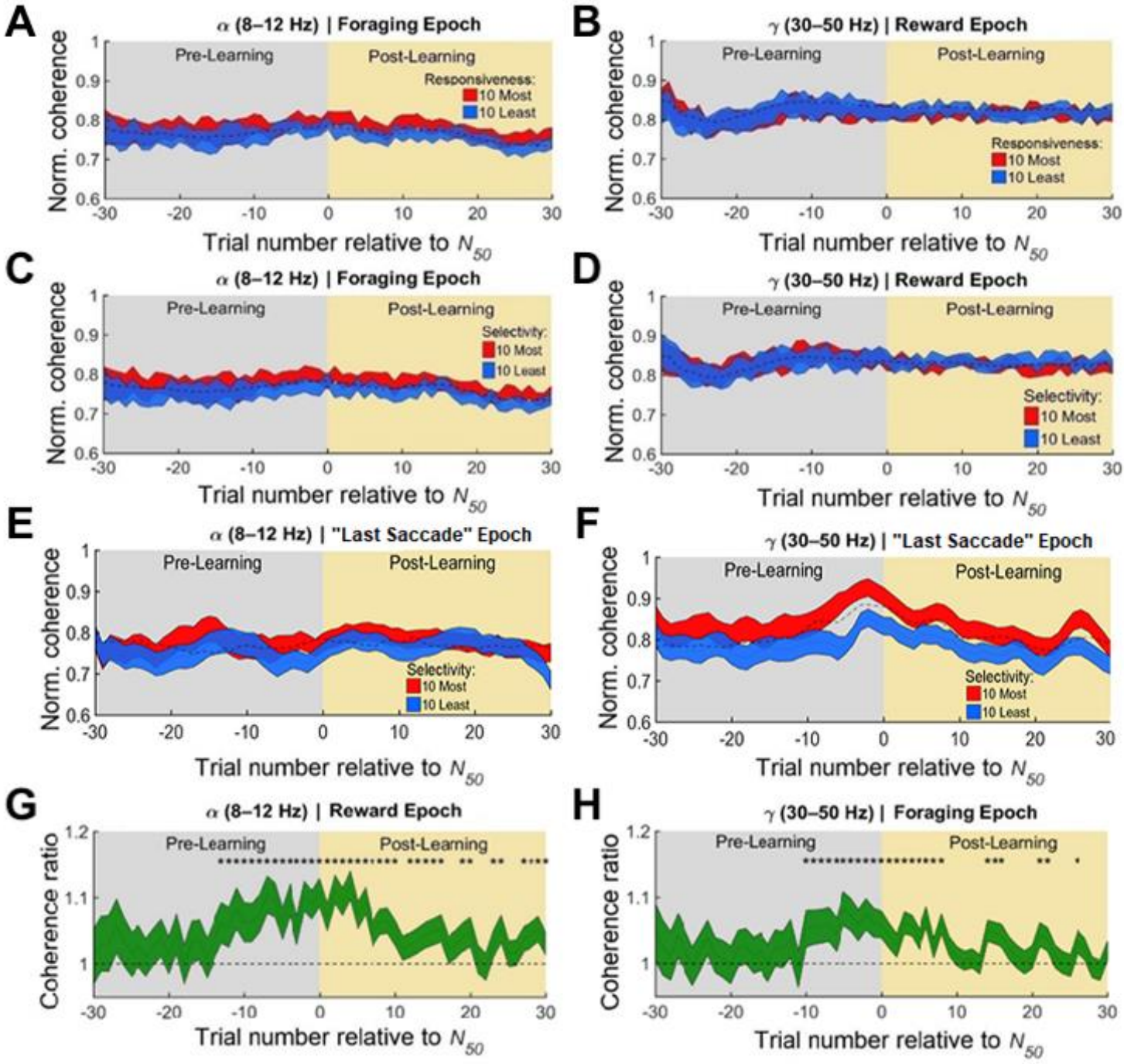
A
α (8–12 Hz) | Foraging Epoch
Pre-Learning
Post-Learning
Responsiveness:
10 Most
10 Least
Norm. coherence
Trial number relative to N_{50}
B
γ (30–50 Hz) | Reward Epoch
Pre-Learning
Post-Learning
Responsiveness:
10 Most
10 Least
Norm. coherence
Trial number relative to N_{50}
C
α (8–12 Hz) | Foraging Epoch
Pre-Learning
Post-Learning
Selectivity:
10 Most
10 Least
Norm. coherence
Trial number relative to N_{50}
D
γ (30–50 Hz) | Reward Epoch
Pre-Learning
Post-Learning
Selectivity:
10 Most
10 Least
Norm. coherence
Trial number relative to N_{50}
E
α (8–12 Hz) | "Last Saccade" Epoch
Pre-Learning
Post-Learning
Selectivity:
10 Most
10 Least
Norm. coherence
Trial number relative to N_{50}
F
γ (30–50 Hz) | "Last Saccade" Epoch
Pre-Learning
Post-Learning
Selectivity:
10 Most
10 Least
Norm. coherence
Trial number relative to N_{50}
G
α (8–12 Hz) | Reward Epoch
Pre-Learning
Post-Learning
Coherence ratio
Trial number relative to N_{50}
H
γ (30–50 Hz) | Foraging Epoch
Pre-Learning
Post-Learning
Coherence ratio
Trial number relative to N_{50}

Figure S3. Specificity of epochs and frequency bands. Related to Figure 4.

(A-D) Normalized coherence between IT and PFC is shown for alpha (8-12 Hz) synchronization during foraging (left column) & low-gamma (30-50 Hz) synchronization following reward (right column). The frequency bands have been swapped across epochs relative to the data shown in Figure 4. Each band represents the grand median of all usable electrode pairs for all images. Error bars display standard error (SEM) across images.

(A,B) Average levels of synchronization, with the data split by *responsiveness* to the appearance of images in IT. For all epochs and bands, there was no statistical difference in the extent to which PFC was synchronized with more responsive (red) and less responsive (blue) sites in IT. The dashed black line indicates the overall average synchronization, which did not change noticeably across trials for these frequencies and these epochs.

(C,D) Average levels of synchronization, with the data split by electrode *selectivity* levels for images in IT. For alpha oscillations during the Foraging epoch and for gamma oscillations during the Reward epoch, there was no statistical difference in the extent to which PFC was synchronized with informative (red) and uninformative (blue) sites in IT. The dashed black line indicates the overall average synchronization, which did not change noticeably across trials for these frequencies and these epochs.

(E-F) Synchronization between IT and PFC is shown for the alpha band (E) and gamma band (F) in the "last saccade" epoch, which consists of the window preceding the saccade into the RZ (225ms to 100ms before the onset of the saccade) . These data shown in the same style as Figure 4. The most selective IT electrodes showed higher gamma synchronization (30-50 Hz) with PFC around the moment of learning in the Foraging epoch.

(G-H) Complementary figures for Figure 4A and Figure 4B:

(G) For Figure 4A, the ratio of synchronization strength for the most and least informative electrodes across trials relative to N_{50}. Asterisks indicate trials in which the ratio was significantly different from 1.

(H) For Figure 4B, as in (G), but for alpha synchronization (8-12 Hz) during the Reward epoch.

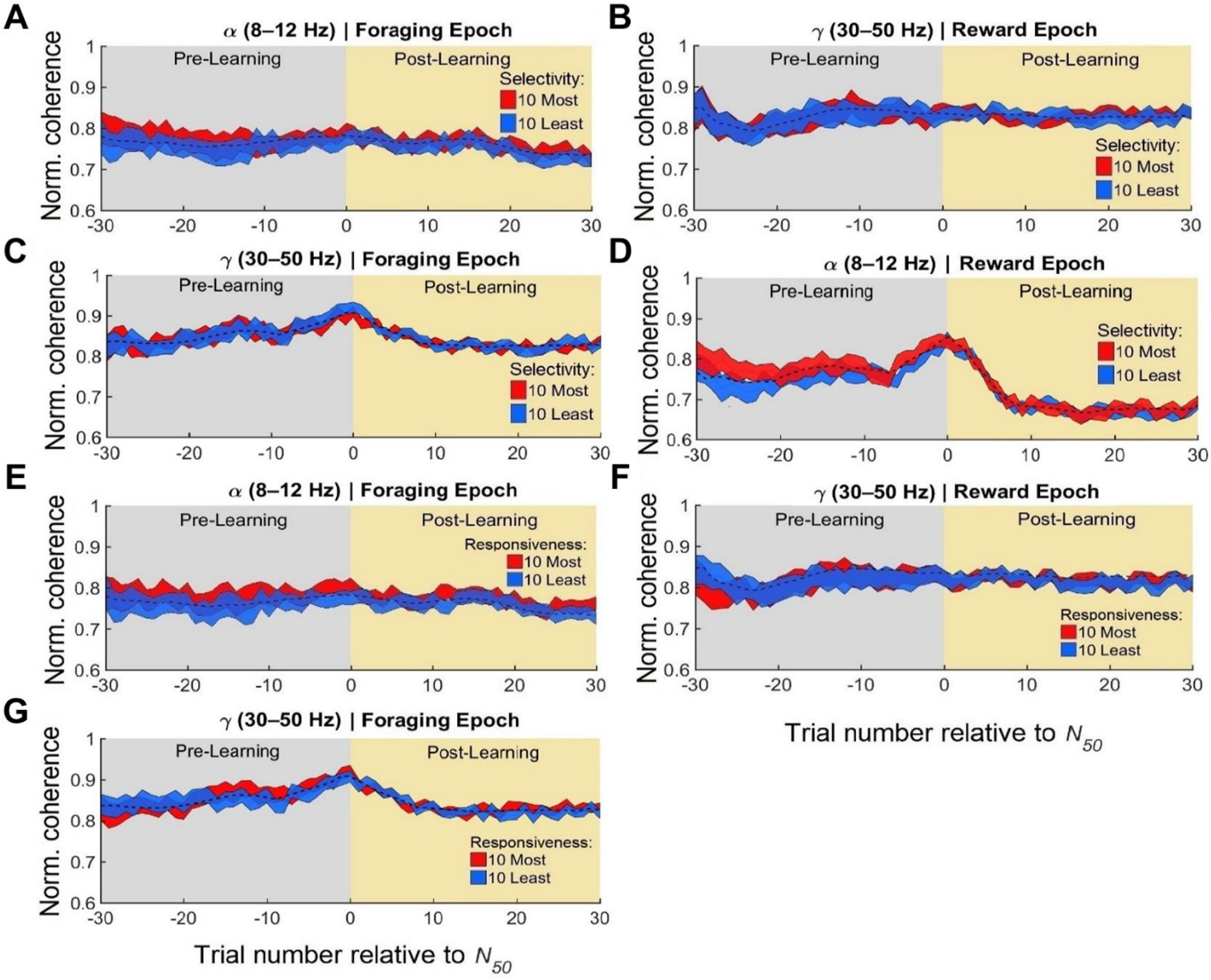
A
α (8–12 Hz) | Foraging Epoch
Pre-Learning
Post-Learning
Selectivity:
10 Most
10 Least
Norm. coherence
B
γ (30–50 Hz) | Reward Epoch
C
γ (30–50 Hz) | Foraging Epoch
D
α (8–12 Hz) | Reward Epoch
E
α (8–12 Hz) | Foraging Epoch
Responsiveness:
F
γ (30–50 Hz) | Reward Epoch
G
γ (30–50 Hz) | Foraging Epoch
Trial number relative to N_{50}

Figure S4. Image responsive or selective sites in PFC do not unilaterally drive synchronization with IT. Related to Figure 5.

Normalized coherence between IT and PFC is shown for during foraging (left column) and low-gamma synchronization following reward (right column) for alpha (8-12 Hz) and low-gamma (30-50 Hz) bands. Each band represents the grand median of all usable electrode pairs for all images. Error bars display standard error (SEM) across images.

(A-D) Average levels of synchronization, with the data split by electrode *selectivity* levels for images in PFC, as using PFC – rather than IT electrodes – to define selectivity. For all epochs and bands, there was no statistical difference in the extent to which IT was synchronized with informative (red) and uninformative (blue) sites in PFC. The dashed black line indicates the overall average synchronization, which did not change noticeably across trials for these frequencies and these epochs.

(E-G) Average levels of synchronization, with the data split by *responsiveness* to the appearance of images in PFC. For alpha oscillations during the Foraging epoch and for gamma oscillations during both the Foraging and the Reward epoch, there was no statistical difference in the extent to which IT was synchronized with more responsive (red) and less responsive (blue) sites in PFC. The dashed black line indicates the overall average synchronization, which did not change noticeably across trials for these frequencies and these epochs.

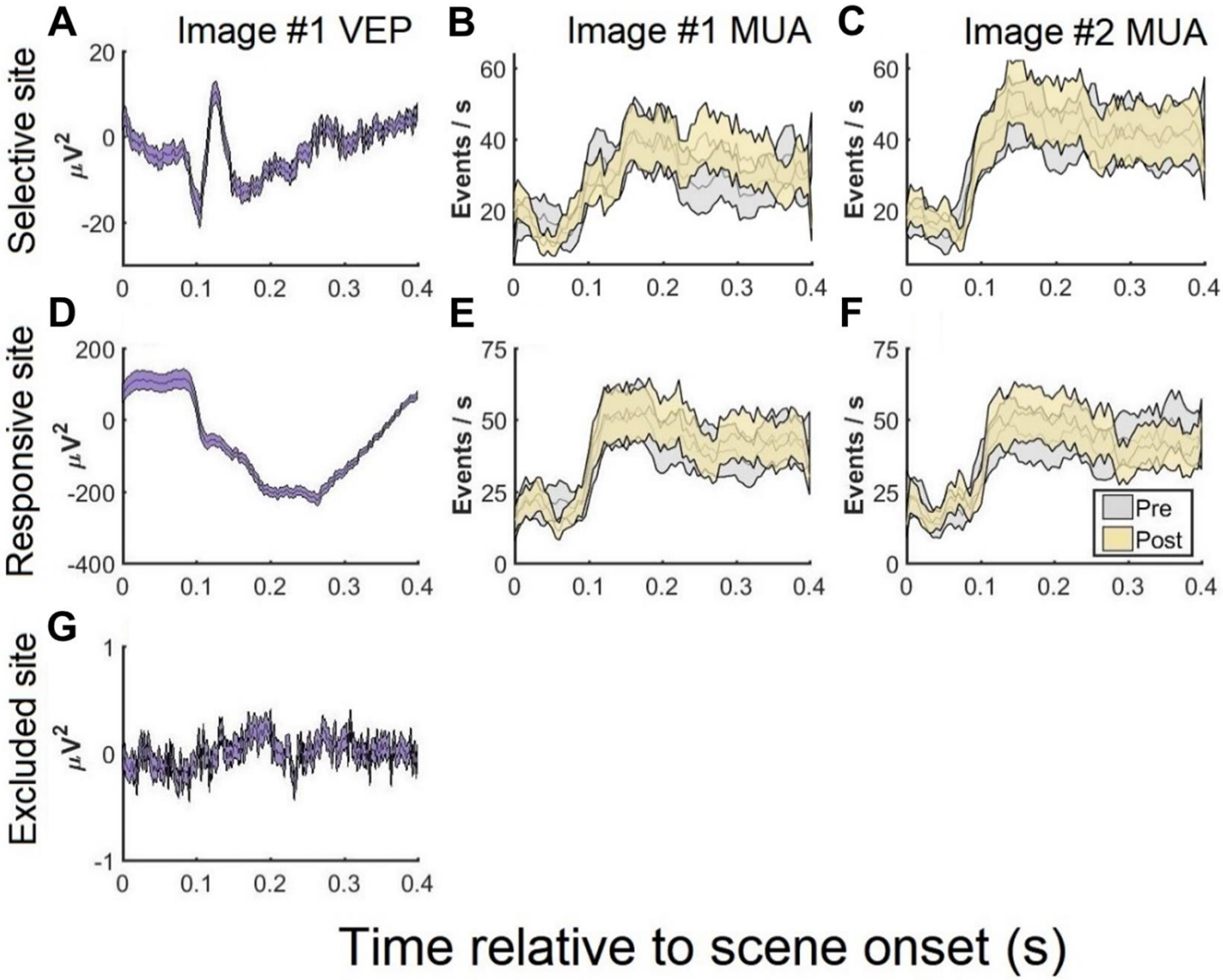
A
Image #1 VEP
B
Image #1 MUA
C
Image #2 MUA
Selective site
Responsive site
Excluded site
μV²
Events / s
D
E
F
G
Pre
Post
Time relative to scene onset (s)

Figure S5. Examples of sensory responses in IT. Related to Figure 7.

(A) Visual-evoked potential from a selective IT channel is shown. The data presented are for the same session used in Figure 1.

(B,C) Multi-unit activity during scene onset is shown for the same channel used in (A) for two images from the same session. Yellow shows the data from the pre-learning phase of the session, while gray shows the data from the post-learning phase of the session. This site responds more to image 2 than to image 1, with no significant change in firing rate or selectivity across stages of learning.

(D) Visual-evoked potential from a more responsive and less selective IT channel are shown. This site responds strongly to image onset but does not distinguish between image 1 and image 2 and does not exhibit significant changes in responses across stages of learning.

(E,F) As in (B,C), but for (D).

(G) An example signal from an excluded IT channel is shown.

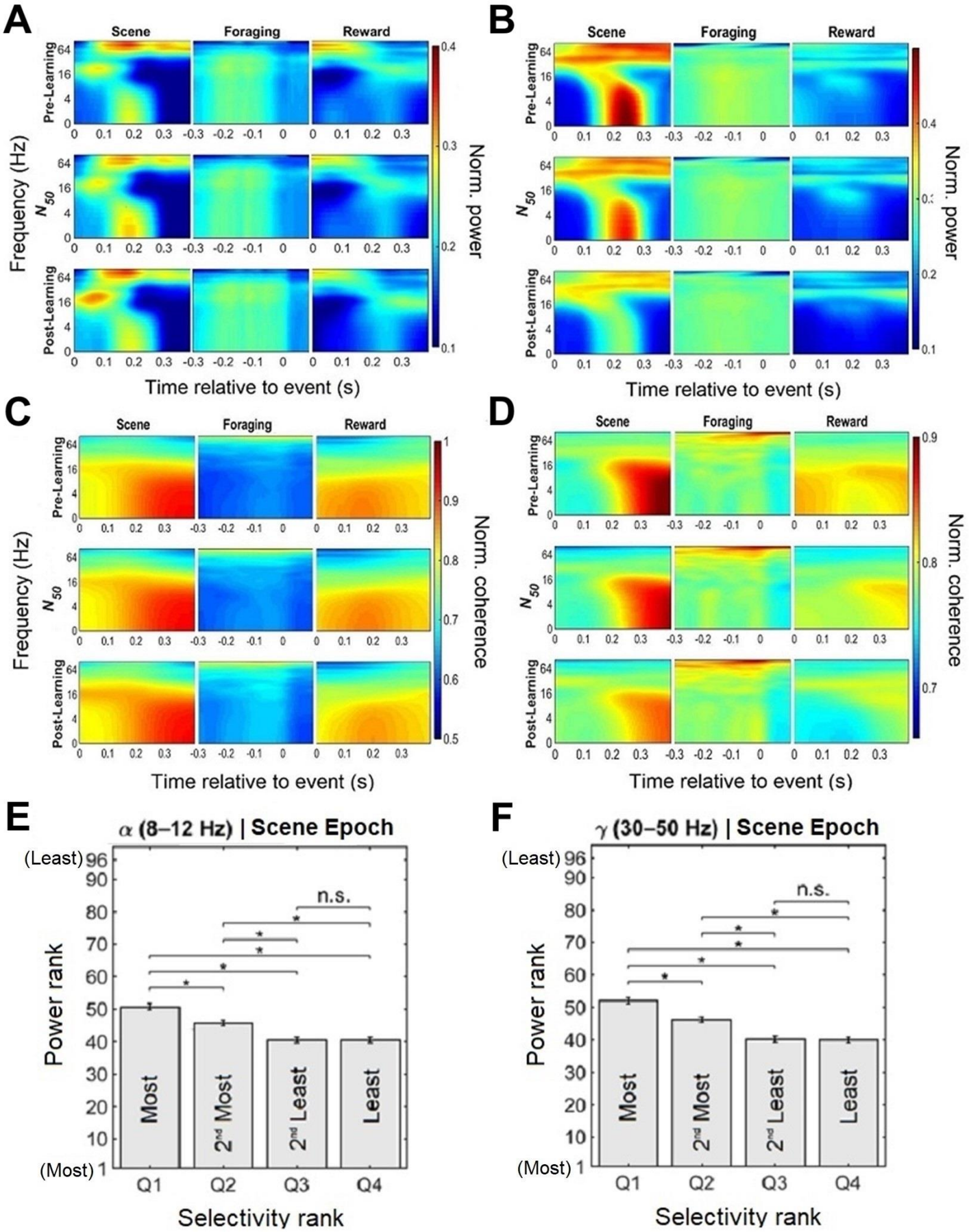
A
Scene
Foraging
Reward
Pre-Learning
N50
Post-Learning
Frequency (Hz)
Norm. power
Time relative to event (s)
B
C
Norm. coherence
D
E
α (8–12 Hz) | Scene Epoch
(Least)
(Most)
Power rank
n.s.
Most
2nd Most
2nd Least
Least
Q1
Q2
Q3
Q4
Selectivity rank
F
γ (30–50 Hz) | Scene Epoch

Figure S6. Abrupt learning is not captured by local LFP power or synchronization. Related to Figure 7.

Time-frequency oscillatory power and coherence (1-100 Hz) for IT (A,C) and PFC (B,D) are shown for three trial epochs ('Scene', 'Foraging', 'Reward') and three stages of learning ('Pre-Learning', 'N_{50}', 'Post-Learning). Learning epochs are binned and metrics are normalized as in Figure 3. Data shown are the grand average of all IT and PFC electrodes for all images for both animals. Reddish colors indicate high power or coherence, while bluish colors indicate low power or coherence.

(A) LFP power in area IT, across all frequencies, time points, trial epochs, and learning stages. The only difference across learning stages was a slight increase in beta (16-24 Hz) power after scene onset (lower left panel), which was confined to the time points earlier than visual response latencies (< 100 ms) and which did not reach statistical significance (two-way ANOVA, $p > 0.05$).

(B) LFP power in area PFC. There was a decrease in low-frequency power (4-12 Hz) during the Scene Onset epoch (two-way ANOVA, $p < 0.05$).

(C) LFP-LFP coherence within IT changed very little with learning.

(D) LFP-LFP coherence within PFC was largely unchanged with learning, except for a modest decrease in the low frequencies (1-12 Hz) from the pre-learning to the post-learning stage of the session (two-way ANOVA, $p < 0.05$).

(E-F) A relationship between IT sites' image selectivity and power was tested for. Electrodes were ranked by their trial-averaged power (in each band individually) during the scene onset period. The results show that there is a very weak (negative) relationship between unit selectivity and power on the same electrodes. To visualize this relationship more clearly, we plot data from animal M, after dividing the selectivity values into quartiles.

(E) Ranking of trial-averaged alpha (8-12 Hz) power versus image selectivity ranking.

(F) Ranking of trial-averaged low-gamma (30-50 Hz) power during versus image selectivity ranking.

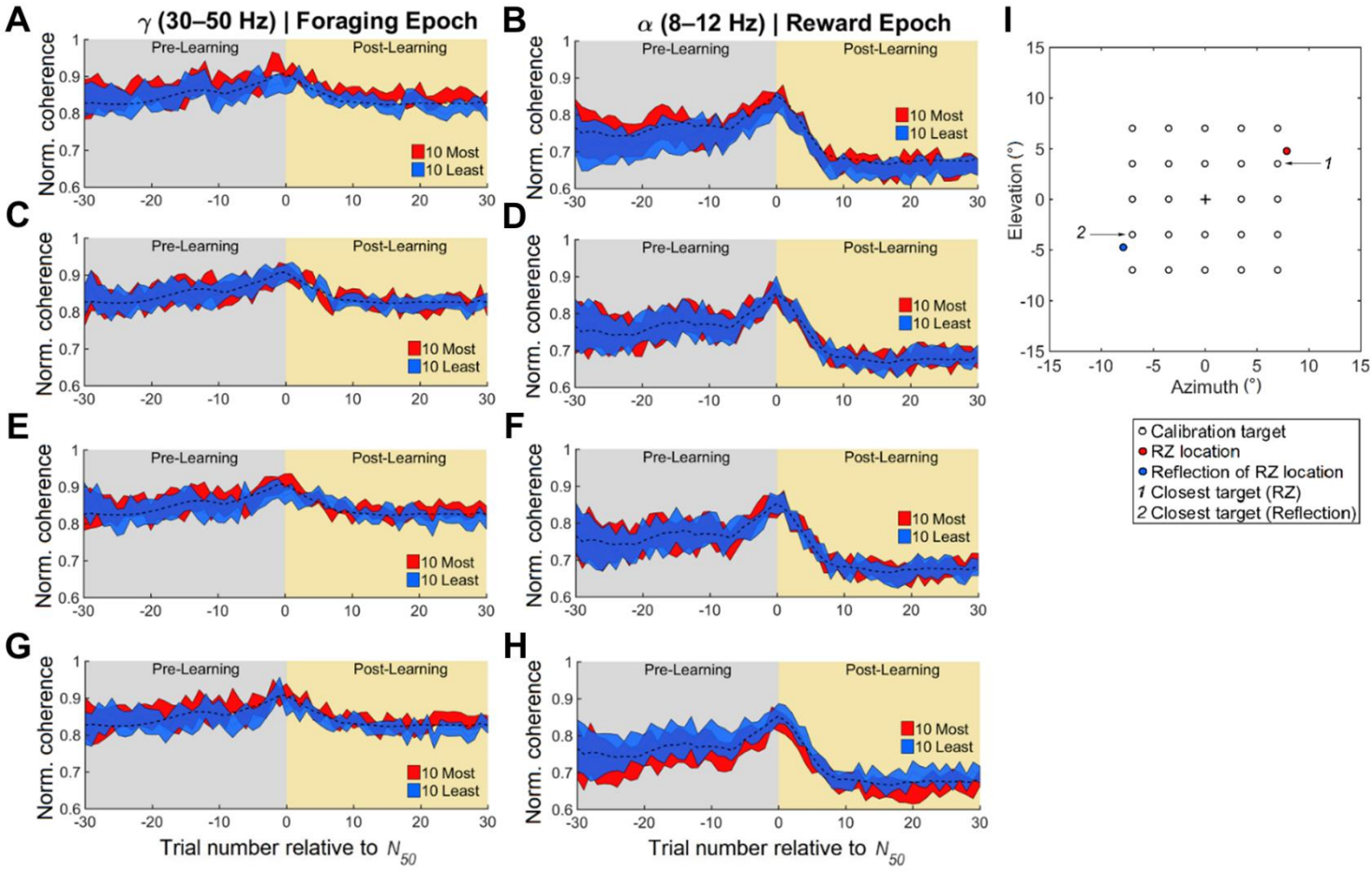
A
γ (30–50 Hz) | Foraging Epoch
B
α (8–12 Hz) | Reward Epoch
C
D
E
F
G
H
I
Pre-Learning
Post-Learning
10 Most
10 Least
Norm. coherence
Trial number relative to N_{50}
Elevation (°)
Azimuth (°)
Calibration target
RZ location
Reflection of RZ location
1 Closest target (RZ)
2 Closest target (Reflection)

Figure S7. Retinotopically selective or spatiotopically selective sites in PFC do not drive synchronization with IT, and vice-versa. Related to Figure 5.

Normalized coherence between IT and PFC is shown for low-gamma (30-50 Hz) synchronization during foraging and alpha (8-12 Hz) synchronization following reward. Each band represents the grand median of all usable electrode pairs for all images. Error bars display standard error (SEM) across images. The dashed black line indicates the overall average synchronization, which did not change noticeably across trials for these frequencies and these epochs. For all conditions, there was no statistical difference in the extent to which informative (red) and uninformative (blue) sites in either PFC or IT synchronized with the other area.

(A,B) Average levels of synchronization, with the data split by electrode selectivity levels for *retinotopy* in PFC, as determined with a selectivity index using multi-unit activity on each electrode.

(C,D) As in (A,B), but with data split by electrode selectivity levels for *retinotopy* in IT, as determined with a selectivity index using multi-unit activity on each electrode.

(E,F) Average levels of synchronization, with the data split by electrode selectivity levels for *spatiotopy* in PFC, as determined with a selectivity index using multi-unit activity on each electrode.

(G,H) As in (E,F), but with data split by electrode selectivity levels for *spatiotopy* in IT, as determined with a selectivity index using multi-unit activity on each electrode.

(I) Diagram of target locations for the calibration task. On every trial, animals made a saccade to a small, high-contrast saccade target, randomly chosen from one of 9 (or 25; illustrated above) locations on a 3x3 (or 5x5; illustrated above) grid spanning the central 14 horizontal and vertical degrees on the monitor. To determine if MUAs encoded the spatiotopic location of the RZ, we matched RZ coordinates (red) and the reflection of the coordinates *(*blue) for each image to the closest target locations in the calibration task. To determine if MUA encoded the retinotopic location of the RZ, we sorted RZ locations according to their positions relative to initial fixation points on each foraging trial, and matched resulting vectors to saccades made in the same (or opposite) direction in the calibration task.